Input Paper prepared for the Global Assessment Report on Disaster Risk Reduction 2015

IMPROVEMENT OF THE GLOBAL FLOOD MODEL FOR THE GAR 2015

Roberto Rudari

Francesco Silvestro

Lorenzo Campo

Nicola Rebora

Giorgio Boni

CIMA Research Foundation

Christian Herold

UNEP - GRID

23/02/2015

Executive Summary

The methodology used for the flood hazard maps derivation encompasses several steps. In defining hazard maps in the "present climate", stream-flow data play a central role. A global database of stream-flow data has been compiled, merging different sources gathering more than 8000 stations over the globe with time series long enough in order to perform a extreme value statistical analysis. Some of these data are daily, but many are collected on a monthly basis. This poor temporal resolution hampers the representativeness of the data for the extreme value analysis. Therefore, such time series have been downscaled using a stochastic technique able to preserve mass and statistical properties at the monthly scale and mimics the statistical properties at daily scale. The algorithm has been extensively calibrated and validated in sites where daily records are available. A statistical regional analysis has been then performed on the daily series in order to compute extreme discharge values in all relevant locations around the Globe. The use of a regionalization technique presents some crucial advantages: the sample size used for estimation increases as time series falling into homogeneous groups can be used together, forming a longer non-dimensional time series thus reducing uncertainty in the estimation of rare quantiles; as a second advantage, the performance of the regression on the geomorphological and climatological variables is expected to improve for the "index discharge" (i.e. a value close to the average of the time series) used to compute quantile values at different locations, in comparison to regression on higher quantiles (resembling extreme events), as the "index discharge" is expected to be more intimately linked to the local climatology and better represented by hydrologic models. A continuous, distributed and physically based hydrologic model was used to improve the regression through the climatological variables and provide insight in location where the "index discharge" is not derivable from observations. Once the discharge quantiles are determined, results are the input of a simplified hydraulic flood model. The model draws hydraulic cross-sections where the flood level is computed from the stream-flow value resolving the manning equation. Levels are then interpolated on the basis of the local relative morphology. On this basic idea several modifications have been introduced in order to take into account of the longitudinal hydraulic connectivity among sections, especially in the large flood plains allowing for braiding of the river and taking into account back water effects.

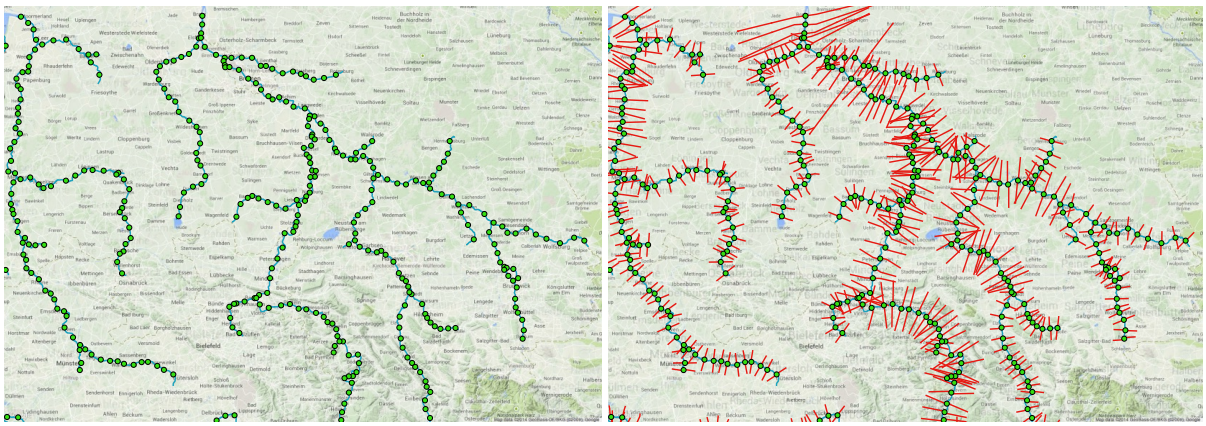

Figure 1 the schematic steps for the flood maps computation: quantiles computation at river sections; Rivers cross-sections delineation; manning equation application and water depths computation.

This first part of the procedure allowed for the determination of the reference Flood hazard maps for different return periods (6 are shown in the global study: T= 25, 50, 100, 200, 500, 1000 years). Such maps have been validated against satellite flood footprints from different sources (DFO archive, UNOSAT flood portal) and well performed especially for the big events. (Figure 2)

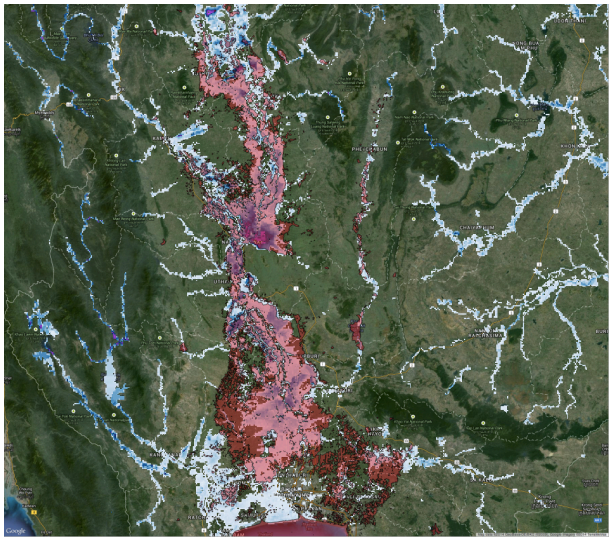

Figure 2 200-year map for Thailand compared with the 2011 Thailand flood satellite flood maps from UNOSAT. Conditioned DEM in the Background.

For smaller events (lower return periods), the GAR Flood hazard maps tend to overestimate with respect to similar maps produced locally (hazard maps where available for some countries and were used as benchmark). The main issue being that, due to the resolution, the GAR flood maps do not take into account flood defences that are normally present to preserve the value exposed to floods. This can influence strongly the results of the risk calculations and especially of the economic parameters. In order to tackle this problem some post processing of the maps has been performed, based on the assumption that flood defences tend to be higher where the exposed value is high and then suddenly drop as this value reduces. Based on the GDP distribution for the different Countries the maps have been post-processed assuming target return periods of the defences as a function of the maximum GDP of the area. In this way the flooded volume have been reduced locally as if

the defences are able to contain the volume for the target return period. The defences are then assumed to partially fail when their design return period is exceed, the failure being larger as the magnitude of the hazard increases.

An initial assessment of the Climate Change influence on flood hazard was performed. In order to study the Climate Change effects on the hazard and risk mapping with regards to floods it was necessary to model all the processes involved in the transformation from rainfall to stream flow. A physically distributed continuous physical model has been applied globally and calibrated on the observed statistics of stream flow. The model was forced with the EC-Earth Global Climatic Model outputs after a bias correction of the temperature and precipitation fields based on global observed grids. The same bias correction is maintained also in future climate. The use of the hydrologic model is two fold: as a future "observation" simulator on which the methodology exposed above is then applied to assess the risk in future climate conditions; in order to derive the correlation structure of the stream flow values in all relevant location in the country. This second element is fundamental in order to simulate a full set of event scenarios with assigned return periods at country level so that it is possible to compute more descriptive statistics on risk: i.e. the full loss exceedence curve. To produce the scenarios multivariate the stream flow distribution simulated by the hydrological model is used to define independent and dependent areas in terms of flooding in each country.

Some interesting results have been found regarding climate change. The problem of assessing extremes in CC is non trivial especially when the hydrologic complexity is added to the atmospheric one. In two hot spots of positive rainfall anomaly (i.e. The Amazon Area and South East Asia), consistently recognized also by IPCC, we obtain two different indications when it comes to discharge extremes. In the first case the hydrologic filter that transforms precipitation into river flow dumps the anomaly and the differences in the extremes are not statistically distinguishable (Figure 3). In South East Asia the result is the opposite and the precipitation anomalies are translated into strong extremes changes, and present extremes statistics can be clearly told from the future one in changed climate. The study used as reference the RPM4.5 scenario as it is considered the most probable so far.

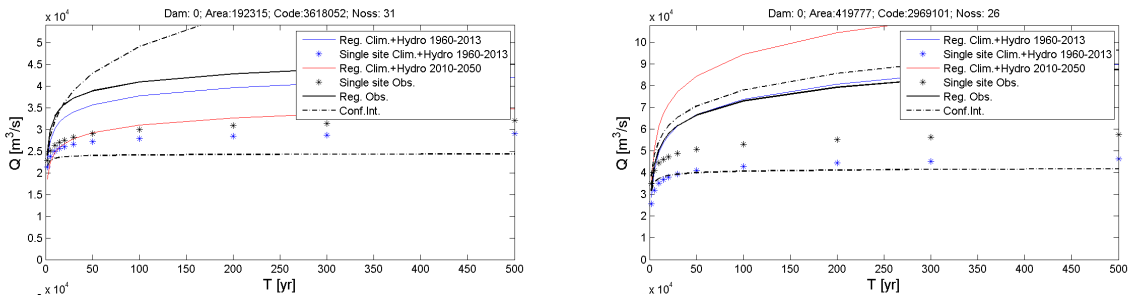

Figure 3 the left panel shows results for the Amazon basin: all curves are contained within the confidence limits; the right panel shows results for one section in the South east Asia domain: in this case the regional curve (in red) falls outside the confidence limits showing a clear increase of extremes frequency.

Background

The Global Assessment Report (GAR) is a major initiative of the UN International Strategy for Disaster Reduction (UNISDR). It contributes to the achievement of the Hyogo Framework of Action (HFA) through monitoring risk patterns and trends and progress in disaster risk reduction and by providing guidance, to governments and non-governmental actors alike, on why and how they can, together, reduce disaster risks. Working as a partnership of UN agencies, international development banks, governments, civil society organisations, universities and expert institutions, the GAR is both a product - in the form of a biennial report published by the UNISDR - and a process of evidence generation and policy engagement**.** This process contributes directly to increasing the effectiveness of disaster risk reduction at the national, regional and international levels.

The GAR process of evidence generation and policy engagement is more critical and urgent than ever for guiding and informing policy making, investment decisions and programming by governments and other stakeholders, contributing *inter alia* to the design of the international arrangements and architecture for disaster risk reduction post-HFA. Its goals are:

1. An enhanced Global Risk Model, addressing gaps in current knowledge on risk patterns and trends and providing accurate and credible information for the global disaster risk reduction community;
2. A significant increase in the availability and quality of data on disaster losses and of metrics for measuring risk, resilience and the cost-effectiveness of risk reduction;
3. Continued and enhanced monitoring of progress by countries and regions against the objectives and priorities for action of the HFA, including through sub-national level assessments; and
4. Policy research on the business case for disaster risk reduction, including scoping studies on pilot industry-led and -agreed standards on disaster risk reduction for a number of key sectors, industries and services.

The present work the first of these goals, i.e. an enhanced Global Risk Model, as it will clearly improve the current Flood Model in several ways.

Global Flood Modelling is one of the targets pursued within the UNISDR Global Assessment Report. The current approach, though valid, has some limitation that can be overcome by incrementally improving the existing model and changing it in some parts.

The process of improving the GFM was a two-step one: the first part completed for GAR 2013 (Herold and Rudari, 2013); the second step completed for GAR 2015 with aim of setting the path for future enhancement of the model itself.

One of the key improvements identified for the GFM resides in having a more robust identification of the quantiles of maximum monthly stream flows on one side as well as providing multiple quantile evaluations referred to different return periods on the other. This final improvement is a necessary precondition for future application of the GFM results to the CAPRA approach.

The 2013 GFM, inter alia, conduct a first draft improvement on Statistical Analysis on Discharge quantile regression, carry out the hazard study from a probabilistic approach, gave strong inputs for vulnerability curves for flooding and improve the output for very localized locations, such as small islands.

However form the results of 2013 it was apparent that further work was to be needed, especially adapting the results obtained so that they could feed appropriately the specific software Platform (CAPRA) to be used by the GAR for the probabilistic risk calculations, and refinement would be needed in order to compute loss curves from hazard maps produced by the Global flood Model.

Moreover the previous work was based on monthly data analysis and do not face the issue of producing statistic for future climate, which are the present grant objectives.

The improvements developed along the following lines:

- Further improvement of the statistical analysis by refinement of the regionalization technique using Daily stream flow data in place of Monthly means.
- As a consequence of the above objective, design of a proper downscaling technique from monthly to daily stream flow data, in order to ensure consistency of the methodology even in places where daily stream flow series are poor or inexistent.
- On the basis of the statistical results, computation of hazard maps for several return periods using a simplified Hydraulic model.
- Implementation of a hydrologic model for stream flow simulations worldwide
- Pre-processing of Global Climate Models outputs (i.e, bias correction and downscaling) in order to feed the Hydrologic model
- Calibration of the Hydrologic model on the statistical analysis on the observed data.
- Hydrological model runs on in climate changed conditions and computation of the stream flow statistics in climate changed conditions
- On the basis of the statistical results, computation of hazard maps in changed climate condition in CC hotspots for several return periods using a simplified Hydraulic model.
- Scenarios implementation for PML and AAL computation in present climate exploiting the Stream-flow correlation modelled by the hydrologic model.

The methodology applied in GAR2011, the starting point of the full improvement process, develops on the following workflow:

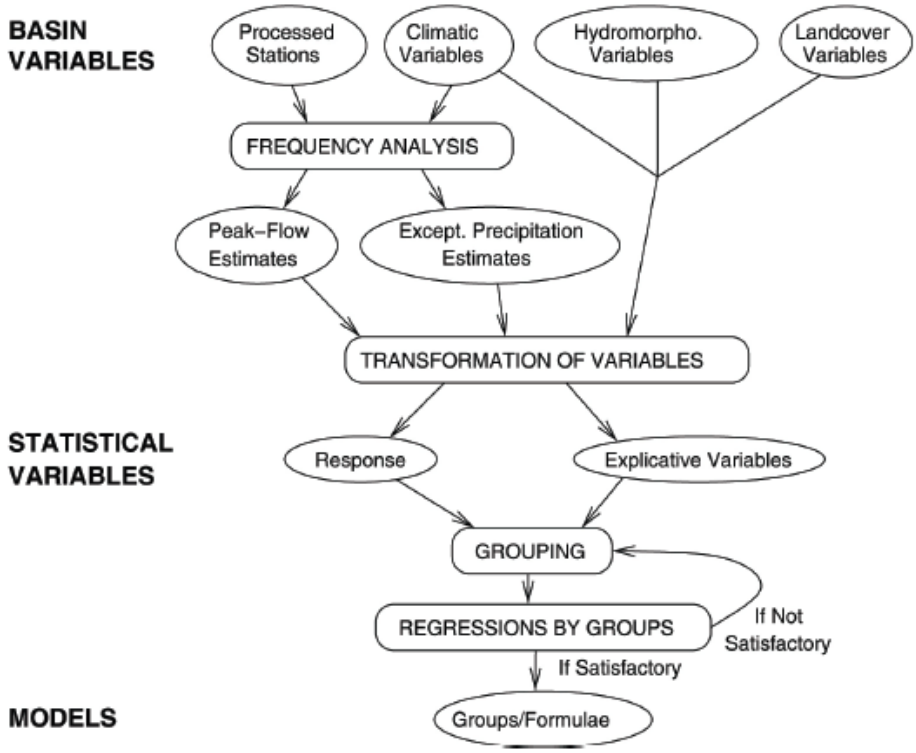

Figure 4 workflow for quantiles determination GAR 2009 & 2011

One of the weak points of this workflow is that the statistical evaluation of the quantiles for assigned return period is done at each single site, where observations are available, and the regression is performed on the quantiles through logarithmic regression on the basin variables. In this way for each return period a new regression is needed to transfer quantiles estimations to sites where observations are not available. Secondly, the robustness of the quantile estimation is dependent on the single site observed time series, which are not often long enough to offer a reliable estimate of rare quantiles. Other improvements could be identified in the simplified hydraulic model used to produce the hazard maps and related water depths especially in large floodplains where the topographic control on the flooded area extension is weak and where backwater effects and braiding of the river might hamper the results of a simplified approach.

The strongest limitation however appears when evaluations in climate-changed conditions are needed. While the 2011 and 2013 methodology heavily builds on observed stream flow statistics which reduces uncertainties in the overall methodology, this hampers the possibility of evaluating future changes in extremes as climate predictions are expressed in terms of meteorological variables such as variations in temperature fields and rainfall patterns. As a result the need of implementing of Rainfall/runoff module arises with evidence. As many choices are possible in tackling this, our choices will be explained in the following paragraph.

Statistical River Flow analysis: Flood Regionalisation

General remarks on the Methodology

The methodology here proposed is based on a different approach that analyzes all statistical data of an identified homogeneous region within the same statistical framework and tries to overcomes both limitations.

Regionalization techniques for discharge quantiles estimation are a common procedure in hydrology (e.g., Basu and Srinivas, 2014; Boni et al., 2007; Mertz and Blosh, 2005). Different approaches exist for Regional Flood Frequency Analysis: e.g. Quantiles Regression Method (QRM), Parameter Regression Method (PRM), Index Flood Method (IFM) (see e.g., Tailor et al., 2011). Each method has advantages and drawbacks. However, the specific advantages offered by IFM are crucial assets in the case of the GFM development that has in its workflow the need to estimate at-site flood frequency with the highest confidence possible even for very low frequency quantiles.

At gauging stations, accepted statistical methods can be applied to evaluate flood discharge magnitude for given probability (see, e.g. Bobe´e et al., 1995; Bras, 1990; Chow et al., 1988). They are usually based on the availability of annual discharge maxima (ADM) time series (in this case on a monthly time window), locally recorded for a sufficient number of years. In other cases, and particularly when records are short, regional analyses are used to extend in time available local observations by merging them in one single time series, with the purpose of increasing estimates reliability especially when low frequency quantiles are of interest (Gabriele & Arnell, 1991; Kottegoda & Rosso, 1997). These methods produce regional growth curves for reduced variables. Working with reduced variables makes the different time series statistically comparable. In case they are proven to come from the same statistical distribution through statistical tests they can be analysed as a single time series having as lengths the sum of the lengths of the single time series. The resulting growth curve counts on a larger sample size.

The so called 'index flood', usually estimated by the ADM expected value based on local observations, is then used to render regional curves dimensional with reference to specific sites. For reasoning on index flood estimation methods see Bocchiola et al., 2003. In un-gauged sites, i.e. sites for which no stage-discharge station and relative records are available, flood frequency can be only estimated by extrapolation of the frequency evaluation made for gauged sites. Since monthly annual maximum probability is of concern, methods used to estimate the magnitude of flood discharges associated with given frequencies can be grouped into two categories. The first collects all methods based on statistical or regression analyses, performed on data pertaining to the same hydrologic region, e.g., recorded ADM at gauging stations, drained area, channel slope, basin shape, location and elevation. Regional frequency analysis belongs to this group. The most diffused regional techniques are the direct regression and the index flood ones (see, e.g., WICP-ACWI, Hydrologic Frequency Analysis Work Group, http://acwi.gov/). The second groups all methods based on the modelling of relevant hydrologic processes, such as rainfall–runoff, flood formation, and flood propagation (Bougthon & Droop, 2003). A combined rainfall-runoff approach is in many cases more informative, especially in river basins with anthropogenic impact. However, due

to the global nature of the work it is difficult to imagine an implementation of this second type at this stage given the time constraints of the overall project, while the first group of methods remains the more straightforward choice.

Within the panorama of regionalization techniques the IFM show advantages that appear crucial in this context. As already stated, sample size used for estimation increases as

homogeneous group time series can be used together forming a longer non-dimensional time series. As a second advantage, the performance of the regression on the basin variables is expected to improve for the expected value compared to higher quantiles (resembling extreme events), as it is expected to be more intimately linked to the local climatology. Climatology indicators can be computed worldwide and can be used to set up the regression. A third advantage is that only one regression on the expected values needs to be computed, while the growth curve (non-dimensional CDF) will remain valid for the statistically homogeneous areas (i.e., Station Groups). In this way, once the index value regression is available any quantile can be derived by the growth curve.

Similar disclaimers with respect to the 2011 implementation hold. As this method is based on large river discharge time-series, it is supposed to represents events that affect corresponding floodplains. The model is not expected to properly represent events triggered in different conditions, for instance costal or flash flooding. The final maps have to give satisfactory results in the case of this new undertaken global risk analysis. It will not provide level of precision required for local analysis or land use planning.

Data Used

River discharge datasets:

As for the 2009 implementation, the discharge station dataset is based on various data sources providing station time-series of monthly mean discharge values. These sources provide various compilations of national or regional station datasets. In places where spatial coverage is still considered as low, some efforts have been made again to obtain data directly from national authorities, but without any successes.

Finally the new dataset is similar to the one used in 2009, except that GRDC recent updates were included in the final compilation.

- Long-term mean monthly discharge dataset. The Global Runoff Data Centre (GRDC), 56002 Koblenz, Germany.
- R-ArcticNET, A Regional, Electronic, Hydrographic Data Network For the Arctic Region. Water Systems Analysis Group. Complex Systems Research Center. Institute for the Study of Earth, Oceans and Space. University of New Hampshire.
- The Global River Discharge Database (RivDIS v1.1). Water Systems Analysis Group. Complex Systems Research Center. Institute for the Study of Earth, Oceans and Space. University of New Hampshire.
- Monthly Discharge Data for World Rivers (except former Soviet Union). DE/FIH/GRDC and UNESCO/IHP, 2001: Monthly Discharge Data for World Rivers (except former

Soviet Union). Published by the CISL Data Support Section at the National Center for Atmospheric Research, Boulder, CO (ds552.1).

- Russian River Flow Data by Bodo, Enhanced. Monthly river flow rates for Russia and former Soviet Union countries in ds553.1 are augmented with data from Russia's State Hydrological Institute (SHI) and a few sites from the Global Hydroclimatic Data Network (GHCDN).
- Discharge of selected rivers of the world. World Water Resources and their use, a joint SHI/UNESCO product. International Hydrological Programme. UNESCO's intergovernmental scientific programme in water resources.

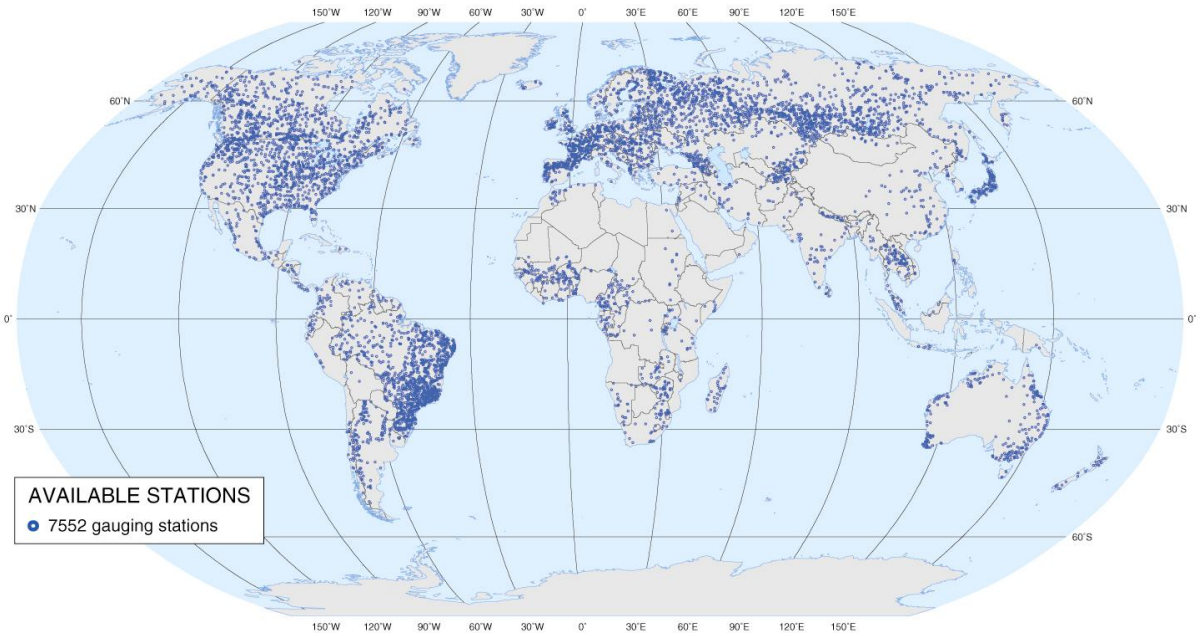

Figure 5 Global distribution of available river discharge stations

Reservoir and Dam Database

The access to a global dam database is essential to estimate the effect of dam networks on downstream river flow.

- The Global Reservoir and Dam Database (GRanD), Global Water System Project (GWSP).

Digital Elevation Model and hydrological derived datasets:

The whole GIS processes are now based on SRTM Digital Elevation Model and other important derived products. The processes and spatial treatments previously based on HYDRO1k Digital Elevation Model (1 kilometer of resolution) show substantial improvement in term of output precision.

- NASA Shuttle Radar Topography Mission (SRTM) SRTM version 2. National Geospatial-Intelligence Agency (NGA) and the National Aeronautics and Space Administration (NASA).

- NASA Shuttle Radar Topography Mission (SRTM) Water Body Data. National Geospatial-Intelligence Agency (NGA) and the National Aeronautics and Space Administration (NASA).
- HydroSHEDS, WWF. In partnership with USGS, CIAT, TNC, CESR.

Land cover datasets:
Land cover dataset are used to generate specific basin characteristics for statistical analysis, and to estimate roughness coefficient required by the hydraulic model as an input parameter.

- Global land cover GLC_2000 version 1. Institute for Environment and Sustainability, Joint Research Centre.
- ESA's global land cover map 2009. ESA/ESA Glob Cover Project, led by MEDIAS France/Postel.
- Global Lakes and Wetlands Database (GLWD). WWF and the Center for Environmental Systems Research, University of Kassel, Germany.

Climatic datasets:
Following climatic datasets are used to generate specific basin characteristics for statistical analysis.

- CRU TS 3.1 monthly precipitation. Climatic Research Unit (CRU) time-series datasets of variations in climate with variations in other phenomena.
- CHIRPS (Climate Hazards Group InfraRed Precipitation with Station data) is a 30+ year quasi-global rainfall dataset. Spanning 50°S–50°N (and all longitudes), starting in 1981 to near-present, CHIRPS incorporates 0.05° resolution satellite imagery with in-situ station data to create gridded rainfall time series for trend analysis and seasonal drought monitoring.
- CRU TS 3.1 monthly mean temperatures. Climatic Research Unit (CRU) time-series datasets of variations in climate with variations in other phenomena.
- Updated world map of the Köppen-Geiger climate classification. The University of Melbourne, Victoria, Australia.

Recorded flood event dataset:
Flood events footprints are used to validate results in term of flood extent for specific return periods.

- World Atlas of Flooded Lands. Dr. G. Robert Brakenridge, Ms. Elaine Anderson. Dartmouth Flood Observatory.
- UNOSAT Archive; http://www.unitar.org/unosat/maps

Data preparation
Standard GRASS hydrological functions are applied on HydroSHEDS digital elevation model to generate the stream network and derivates layers. Geographic projection is not modified but a real surface raster, based on an ellipsoid, is used during these treatments to maintained real drainage area in the various outputs. This real surface raster is used when needed in subsequent spatial analyses to avoid re-projecting layer in an equal-area projection.

Stations are individually adjusted on stream network comparing recorded and modelized drainage area values. When a difference threshold between these two values is reach, the station is considered as situated on the right stream section. This treatment is essential for establishing spatial correspondence between river stations as recorded in a database, and the digital elevation model and its derivates hydrological layers. Additionally, this process allows excluding some stations, in case of duplicates or inappropriate location on the stream network.

A similar procedure is applied on dam database in order to better fit the dam point to the adequate stream section.

Each station drainage basin is then characterized by a set of variables based on above described global datasets:

Hydromorphometric:

- Drainage area
- Mean basin elevation
- Mean basin slope
- Basin shape
- Main channel length
- Main channel slope
- Drainage frequency
- Distance to final outlet

Land cover:

- Surface water storage
- Forest cover
- Impervious cover

Climatic time-series:

- Mean annual precipitation
- Temporal mean of monthly maximum precipitation
- Minimum mean monthly temperature

Climatic zones:

- Percentage area of Köppen-Geiger climatic zones

Upstream dam network:

- Dam characteristics
- Temporal mean of monthly maximum precipitation in dam network catchment

Flood Frequency analysis implementation

Downscaling of stream flow data

A large number of applications requires the availability of streamflow data at a detailed temporal resolution: water supply reliability, reservoir operations, management of water resources, analysis of low frequency flow. In many case historical series are made by data at low temporal resolution (e.g. monthly) (Smakthin 2000) and only a subset of available stations have generally data at higher temporal resolution (e.g daily). In another number of cases for the same stations older data are at coarse resolution while recent data are at higher resolution, for example because sensors are changed or automatic data transfer systems have been installed. Looking for example at number of global or country available data sets it can be discovered that in many cases only monthly data are available.

For these reasons the need to downscale streamflow data arises, especially for selected type of scopes, for example the statistic studies of extreme values or water management. There is a wide range of basin categories for which carrying out extreme statistical analysis on daily data is reliable since yearly maximum daily flow is good quantitative indicator of the instantaneous peak flow, while maximum daily and monthly flow are not negligibly different.

Many methodologies have been presented in previous works with the aim to disaggregate in space and/or in time annual to seasonal flow, seasonal to sub-seasonal flow, monthly to daily flow. We can cite for example, Lane (1979), Salas et al., (1980), Koutsoyiannis and Manetas (1996), Lall and Sharma (1996) and Tarboton et al. (1998).

Many of these techniques are quite complex and need optimization techniques to be applied, in various cases they also need iterative processes that could be computational demanding (Koutsoyiannis, 2001; Prairie et al., 2007).

Here we propose a method that follows an autoregressive approach (Rebora et al, 2006). It is made by a filtered auto-regressive model able to generate possible daily streamflow time series using monthly data as input. The algorithm has a stochastic term that allows to produce a number of possible daily flow time series that all maintains the volumes at monthly time scale of the input data. It is easy to implement and not computational demanding, it can be useful especially when high temporal resolution (e.g. daily) time series need to be generated without the constrain of spatial disaggregation (example: statistical analysis).

In the following we report the steps needed for generating high-resolution, likely, daily discharge starting from monthly averages.

1) We estimate the slope of the power-spectrum of the Q(T) time series. To do this we obtain the Fourier transform of Q(T) whose power spectrum is indicated as $\left|\widehat{Q}(\Omega)\right|^2$ $\left|Q(\Omega)\right|^2$ in Fourier space (reported as a blue line in Figure 6).
2) We then generate a power spectrum indicated by the red line in Figure 6 whose spectral slope is defined according to the power law $\omega \sim \omega^{-\beta}\, \omega \approx \omega^{-\beta}$ and whose b values can ranges from 3 to 1. b represents the first free parameter of the model.

3) As a third step we generate the Fourier spectrum by adding uniformly and randomly distributed Fourier phases. The result is as follows: $\hat{g}(\omega) = |g(\omega)|e^{i\phi(\omega)}$. We use the small letters and change the name to the variable since now the signal has increased the time resolution (from monthly to daily, even if in Fourier space) according to the power law $\omega \sim \omega^{-\beta}$ (red line in Figure 6). By inverting the Fourier spectrum we obtain a gaussian field in physical space: g(t) with a daily time resolution but gaussian values.
4) We then generate a daily discharge time series by exponentiating the gaussian field according to the exponential law: $\tilde{q}(t) = exp\,\alpha[g(t)]$ whose a values can range between 0.5 and 2 and a represents the second free parameter of the model.
5) As last step we force the discharge values $\tilde{q}(t)$ of the generated daily discharge time series to be equal to the series Q(T) when aggregated at a monthly scale. This give us the guarantee that each daily time series is equal to the monthly time series if averaged at this scale. This results in the following operation: $q(t) = \tilde{q}(t)\frac{Q(T)}{\tilde{Q}(T)}$ where $\tilde{Q}(T)$ represents the time series $\tilde{q}(t)$ averaged at monthly scale.

The parameters a and b are then obtained by minimizing the differences between the original daily duration curves and those obtained by downscaling the monthly time series.

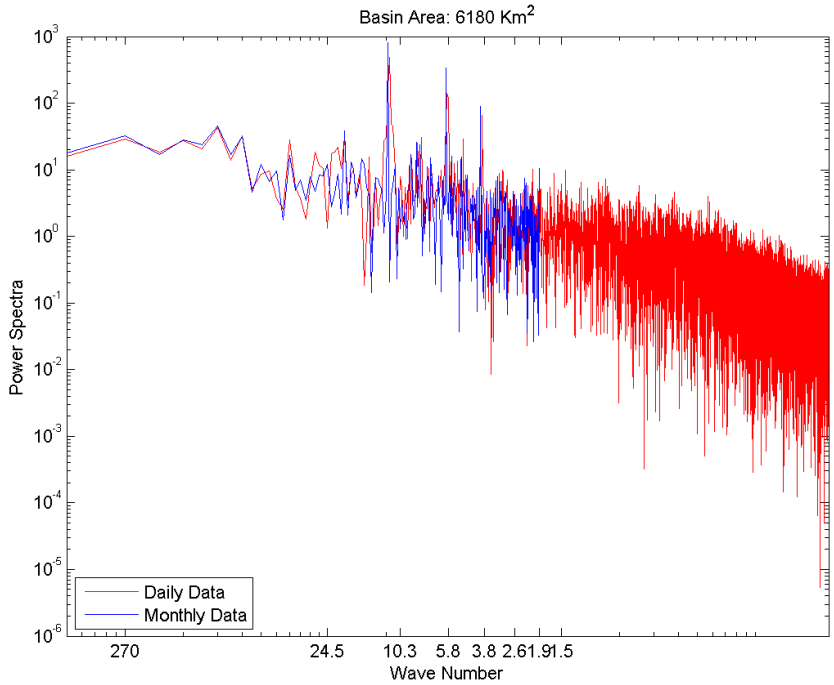

Figure 6 power spectrum for a daily time series and for the corresponding monthly time series.

The proposed model is able to take into account differences into average monthly stremflow due to the changes of discharge regimes (e.g. introduction of a dam).

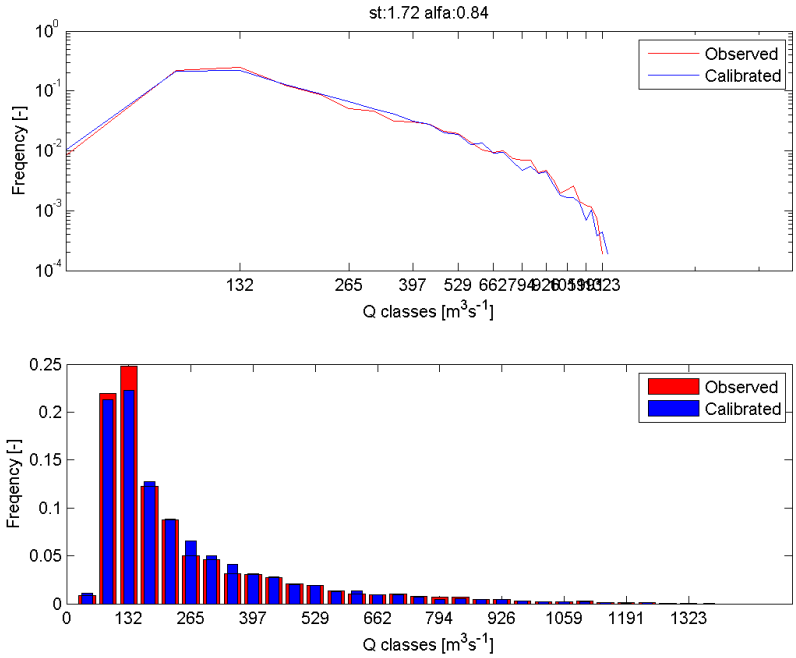

Figure 7 shows the comparison between observed and simulated power spectra of streamflow.

The method has been applied on the full data set with good results in terms of duration curves reproduction and even of hydrographs modeling. Considered stations have an upstream drainage area that covers a wide the range and they are located in zones with different climatology (Peel et al., 2007).

Single site distribution fit and choice of the "parent" distribution

The first step in the methodology implementation is to identify a proper statistical distribution for the description of the single site data and the growth curve after that. Various distributions have been considered parent distributions and several distribution fits were performed on the different gauged stations with reasonably long time series (see e.g. Figure 2). Eventually the choice fell on the GEV distribution (see e.g., Hoskin and Wallis, 1993), that scored better in the overall distribution fit exercise and represent a good compromise between flexibility and robustness. The main reasons for this choice can be summarized as follows:

- It is widely used for the description of extreme values of physical processes (Katz et al., 2002)
- It has three parameters and therefore allows for a good flexibility so that can it be adapted to a large casuistry of observed distributions
- It is easy to implement since an explicit formulation of the quantiles exists

The Cumulative Distribution Function (CDF) is given by the following equation:

$$F_X(x) = \Pr[X \le x] = \exp\left\{-\left[1 - \frac{k(x-\varepsilon)}{\alpha}\right]^{1/k}\right\}$$

Where k, α, ε represent respectively the shape, position and scale parameters.

The GEV distribution fit is carried out on each site where a reasonable length of the sample is available. After an analysis of the available samples we considered N=20 as the minimum number of years of data.

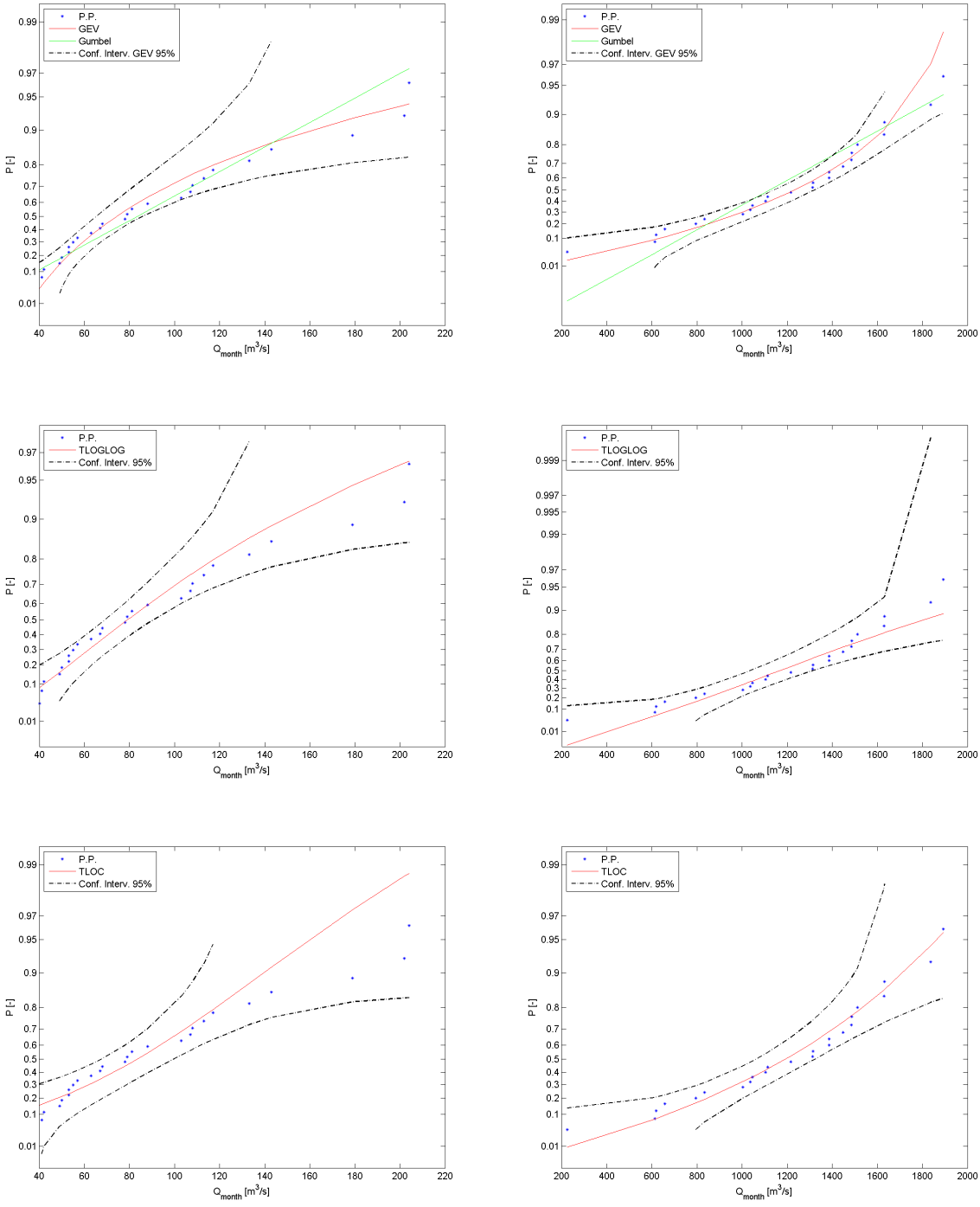

Figure 8 Different at site distributions fit to data. Here a comparison for two stations and some statistical distributions is shown.

Figure 9 shows the curve together with the data for different stations, the confidence intervals are also reported. The four sections are located in North and Central America. It is evident that in single site estimations for quantiles above .9-0.95 the confidence intervals

tend to explode, providing a very uncertain estimation of the T=100 years quantile and above.

When the regionalization approach is used and the growth curves are considered this problem is considerably smoothed out. This will be clearer in the following paragraphs.

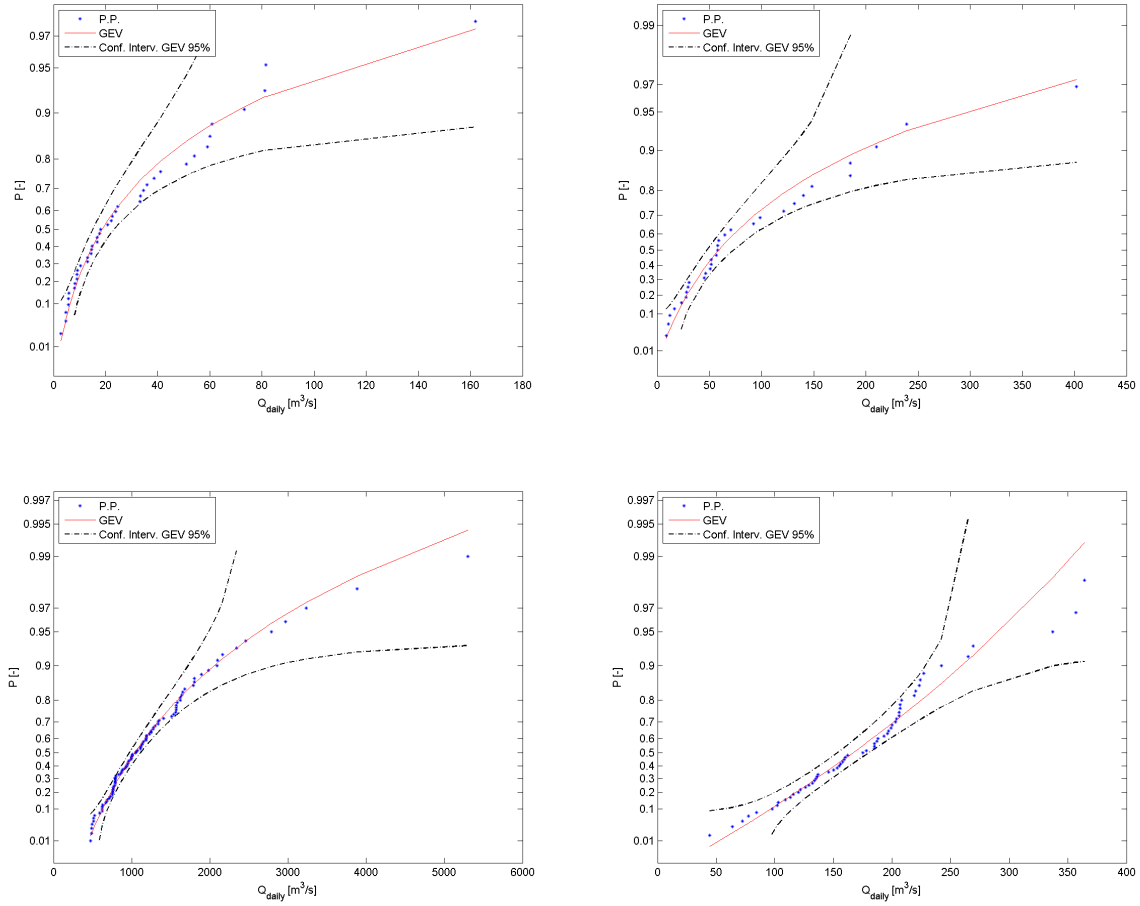

Figure 9 Distribution fit to data for different stations; Gev distribution

Identification of the homogeneous regions

The homogeneous regions identification is the most difficult, and less objective step of the regionalization procedure. In this study they have been determined starting from considerations and analysis about climatology and hydrological regime of the basins pertaining to the region.

As a start the Köppen Geiger (KG) classification (Peel et al., 2007) has been used to identify the main climate zone of the considered area. Five primary classes from the KG classification have been considered: Tropical, Arid, Temperate, Cold and Polar as depicted in Figure 10.

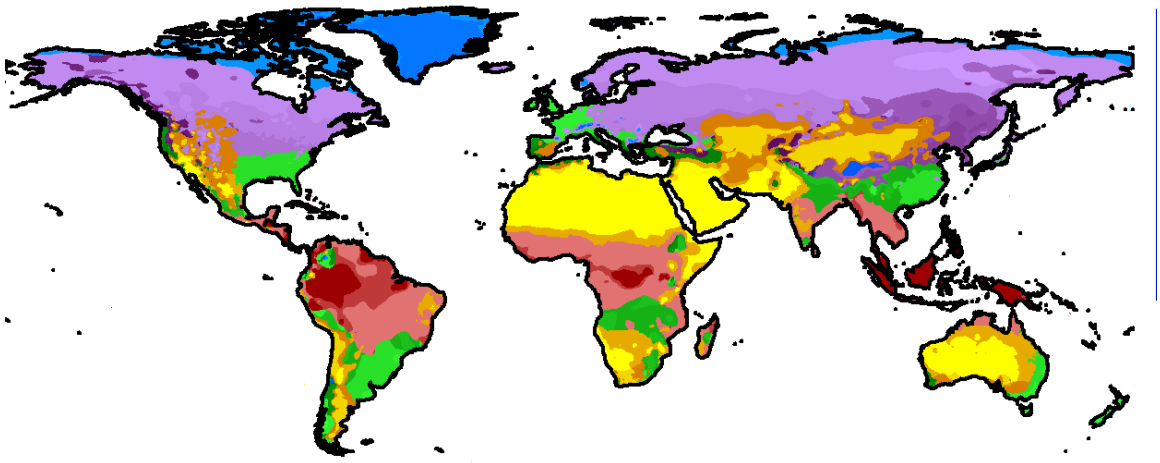

Figure 10 Map of Köppen Geiger climatic zones classification: tropical in red tones, temperate in green tones, arid in yellow tones, cold in violet tones and polar in blue tones.

This classification has been used as main driver of the final classification. The classification need to modified as it does not refer to consistent hydrologic units, namely basins and sub basins. The hydrologic response of the basins and as a consequence on its rain regimes has to be considered. In fact, basins that are on different climatic zones might show a similar behaviour in terms of hydrologic response, especially when they are located in transition areas between two main climatic zones. On the other hand, the same climatic zone can have sub-zones with different rain regimes, these differences are due not only on the different precipitation amounts that occur on predefined temporal windows (e.g. 1 year, 1 month), but also on the variability of these amounts. This can reflect in a noticeable variability of the hydrologic response. Hydrologic response variability is a key factor in homogeneous zone identification.

The variability of the hydrologic regime can be synthetically described by the Coefficient of Variation[1] (CV) of the maximum flow series. High values of CV indicate that there is a high variability of data values that can be very different from one year to another. This parameter can give indication of the driving rainfall regime of the area as arid climates are expected to show more variability than humid climates.

In Figure 11 the map of CV obtained by interpolation of the stations the CV is reported

By comparing Figure 10 and Figure 11 it can be notice that in many cases that pattern of CV follows the climatic KG classification. As an example it is evident how the arid zones are often characterized by high values of CV. It is nevertheless evident that other cases this correspondence is much less clear as the hydrologic interactions are more complex, as an example the north coast of Black sea as well some areas of Siberia show high CV but they are in cold climatic zones and that is of no trivial interpretation.

[1] CV is expressed as the ratio between standard deviation and mean of the data series
[2] http://www.cgiar-csi.org/data/srtm-90m-digital-elevation-database-v4-1
[3] http://floodobservatory.colorado.edu

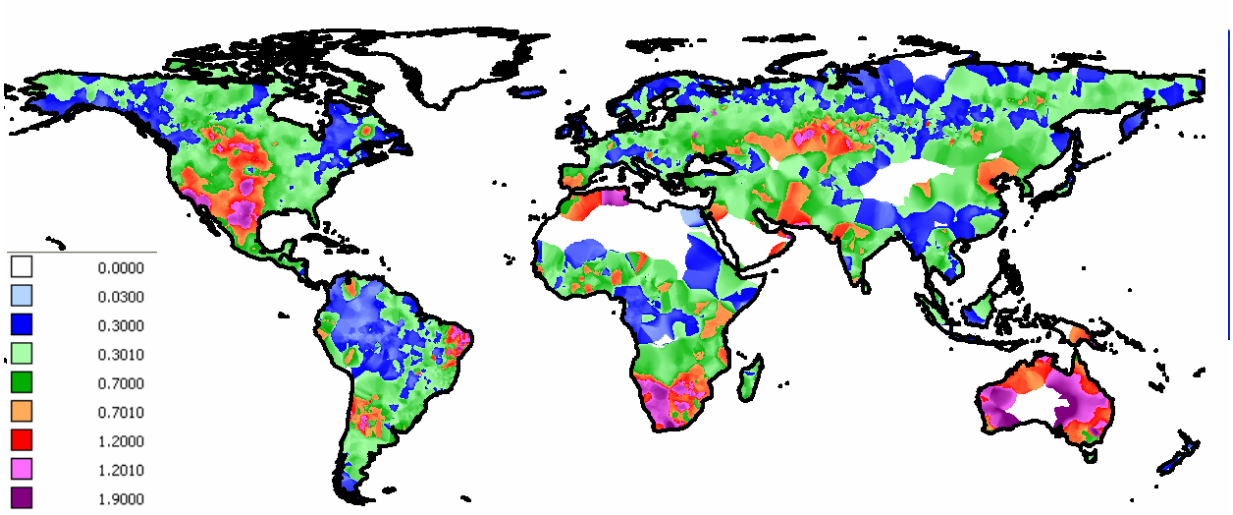

Figure 11 Map of coefficient of variation of the maximum monthly flow

This is confirmed by the analysis carried out following the work of Burn (1997) and is summarized in Figure 12. The 12 sectors represent the months of the year while the distance from the centre of the circle is a function of the CV value: the closest the point to the centre the smaller the CV value, the closer to the circle the higher the CV. The graph is built using the data of the North Hemisphere.

The points have different colours according to the KG climatic area. The Climatic area is assigned to the section analyzing its upstream catchment. The climatic area with the maximum percentage of area of the catchment is considered as the dominant area at this stage (if a basin belongs for the 30% to tropical and 70% to temperate is classified as temperate).

The graph shows the distribution of the Maximum Streamflow data along the year and their variability; it is quite evident that arid basins have generally high values of CV, the temperate and cold zones have a pronounced seasonality, concentrating the Maximum Streamflow data in well defined periods of the years

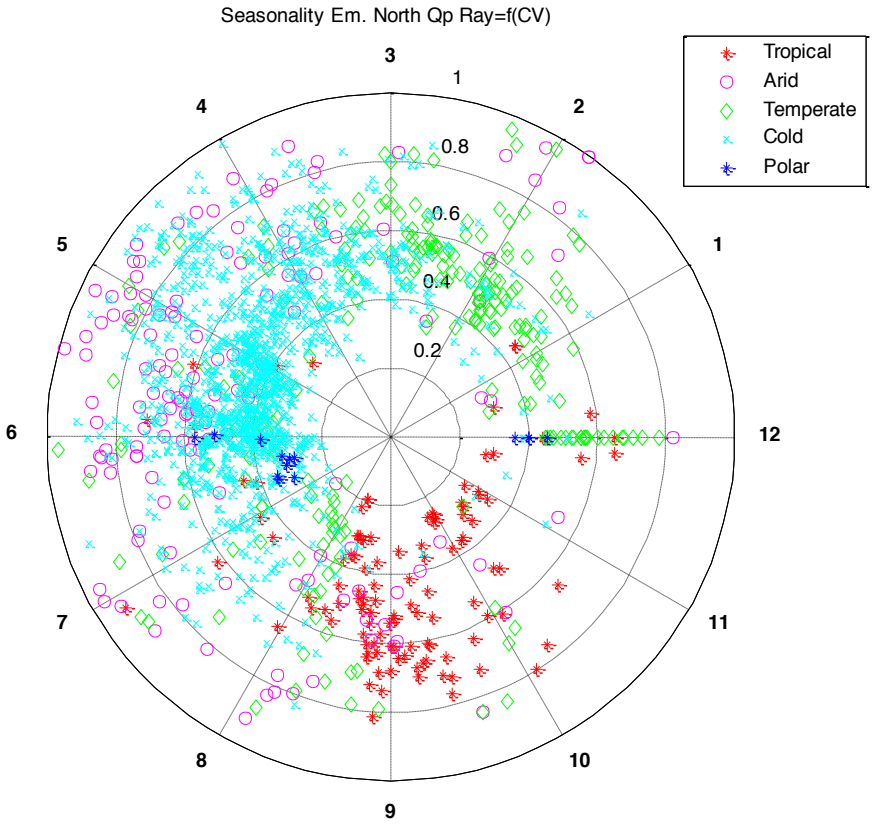

Figure 12 Seasonal and CV spatial representation Map for the stations of the North Hemisphere.

Finally, to maintain as often as possible the homogeneity at basin scale, we tried to avoid designing homogeneous regions that cross the basins. This is evidently not always possible, especially when large basins that cross-regions that have very different climatology and precipitation regime are considered.

Summarizing, three main criterions have been followed to identify the homogeneous regions:

1) the Köppen Geiger climatic classification;
2) the rain regime of the region, minimizing the CV variability in the region;
3) minimizing the number of basins that belong to more than one homogeneous region.

The naming of the homogenous regions is given basing on the following rules:

- the first number indicates the main continent;
- the second number the main climatic zone;
- the third number the sub zone (if existing).

Continents:

1:North America; 2: South America; 3: Europe; 4: Africa; 5: Asia; 6: Australia.

Climatic zones:

1:Tropical; 2: Arid; 3:Temperate; 4:Cold.

Example:

Region 531; 5:Asia; 3: Temperate; 1: first Sub-Region

A unique polar zone has been considered for the entire world.

Final Section assignment to homogeneous regions.

The problem of assigning a certain section along the stream network to a homogeneous region is of concern when the river crosses more than one homogeneous region. These region are delimited by geographic boundaries and it is not infrequent that the upstream basin of a certain section lays for its larger part in a different region in respect the region of the section.

We needed an automated procedure to assign each section to a homogeneous region. The easiest way would be to assign the region where the largest part of the upstream basin pertains (as done in the first step). However, the hydrological behaviour in terms of discharge is in fact strongly influenced by those parts of the basin where the largest amount of precipitation is collected.

The adopted methodology is therefore the following.

Be A1, A2,..Ai…An the part of drainage area A of a certain basin closed in the section s that crosses the homogeneous regions 1,2,..n.

Be P1, P2,..Pi…Pn the mean annual precipitation occurring in the areas A1, A2,..Ai…An as derived from observations.

The homogeneous region assigned to the section s (HR_s) is the one that satisfies the equations:

$HR_s = imx$ with imx such that $P_{imx} * A_{imx} = \max(P_i * A_i)$.

Once the homogeneous regions are defined all stations pertaining to that area are grouped, rendered dimentionless so to build a time series. On the basis of the time series it is possible to estimate the parameters of the GEV and build a growth curve of the area that describes the growth factor. An example is given in Figure 13 where a detailed comparison is given between the Monthly Growth curve, the Daily Growth curve derived from observations and from reconstructed daily values as per the procedure described in section 0. A strong difference, statistically significant as evident from the confidence limits, is present between Monthly and Daily curves, while the two daily ones are statistically indistinguishable. Figure 9 shows a synoptic overview of growth curve fit to data for the different homogeneous region

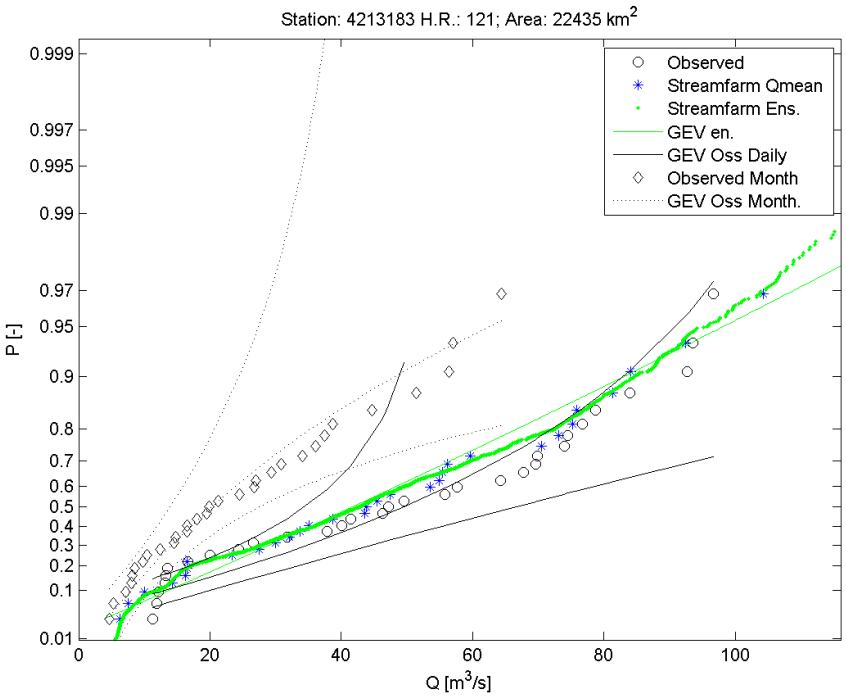

Figure 13 Example of growth curve fit to data - GEV distribution. The figure shows observed monthly and daily data. Growths curves from monthly, daily observed and daily simulated data are also compared.

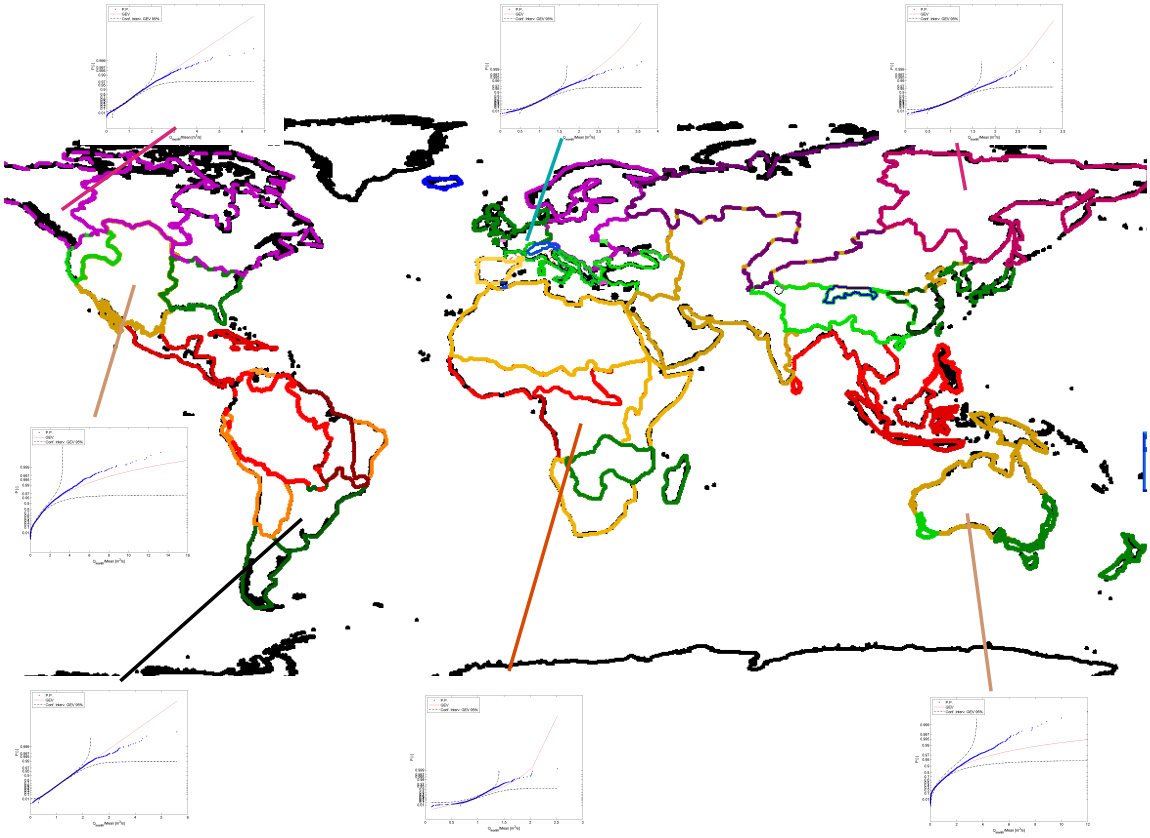

Figure 14 Synoptic overview of growth curve fit to data for the different homogeneous regions.

Homogeneity testing

Dalrymple (1960) recommended a test which compares the variability of 10-year flood estimates from each site in the region with that expected if sampling error alone were responsible for between site differences. There have been several applications of this test: Dalrymple (1960) in Pennsylvania and Maryland, USA; Cole(1966) in England and Wales; Biswas & Fleming (1966) in Scotland; and Chong & Moore (1983) in Illinois. In these applications the regions being studied have been found in each case to be homogeneous suggesting either that the test may not be particularly powerful or that a wide variety of flood series and of basin types is consistent with homogeneity.

A more powerful statistical test will involve homogeneity of the analysed region in terms of higher order moments such as CV and Skewness. Particularly, a homogeneous flood frequency region will contain annual maximum monthly flow populations whose flood frequency relationships have similar slopes on a probability plot. Therefore, variations of Coefficient of Variation (CV) and Skewness (Sk) should be attributed only to sample size limitations. This could be tested via Montecarlo simulations once the parent distribution (growth curve) have been computed. In the specific, series of sample size similar to the observed ones are created from the parent distribution and then treated as observations. A Chi Square test is then used to test if the observed distribution of CVs and Skewnesses can be statistically distinguished from the synthetic one. If they cannot distinguish it is assumed that the observed data can be generated by the same parent distribution and therefore the homogeneity test is passed. The homogeneity test was passed without problems by many initially identified regions (Figure 15 -Figure 16), while others need to be divided in to sub-groups to pass the test, thus refining the homogeneous areas identification.

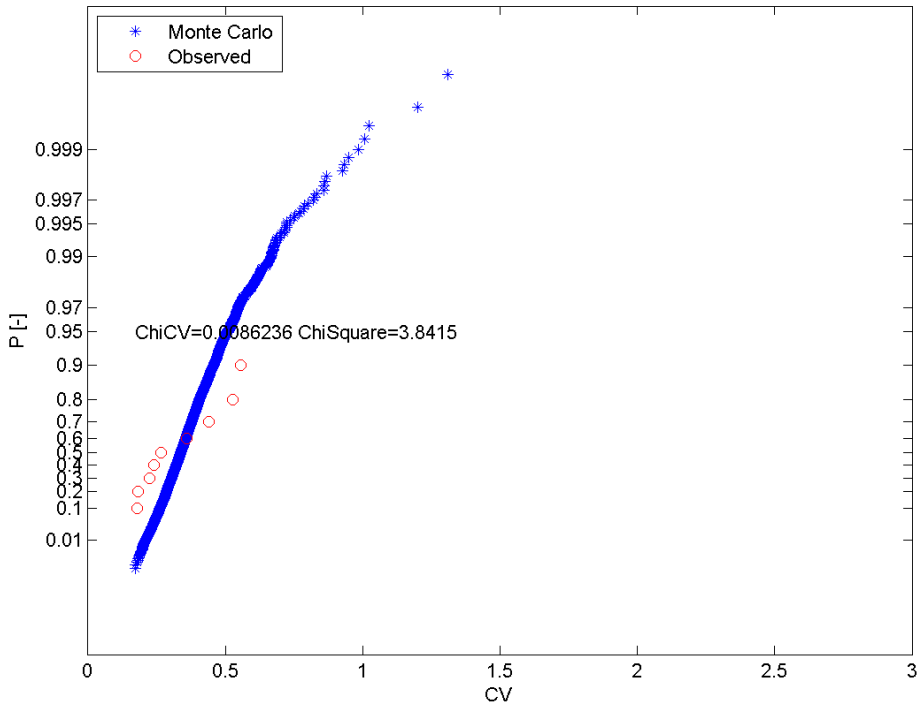

Figure 15 Example of homogeneity Chi Square test for the Coefficient of Variation by means of Montecarlo technique. Gev distribution

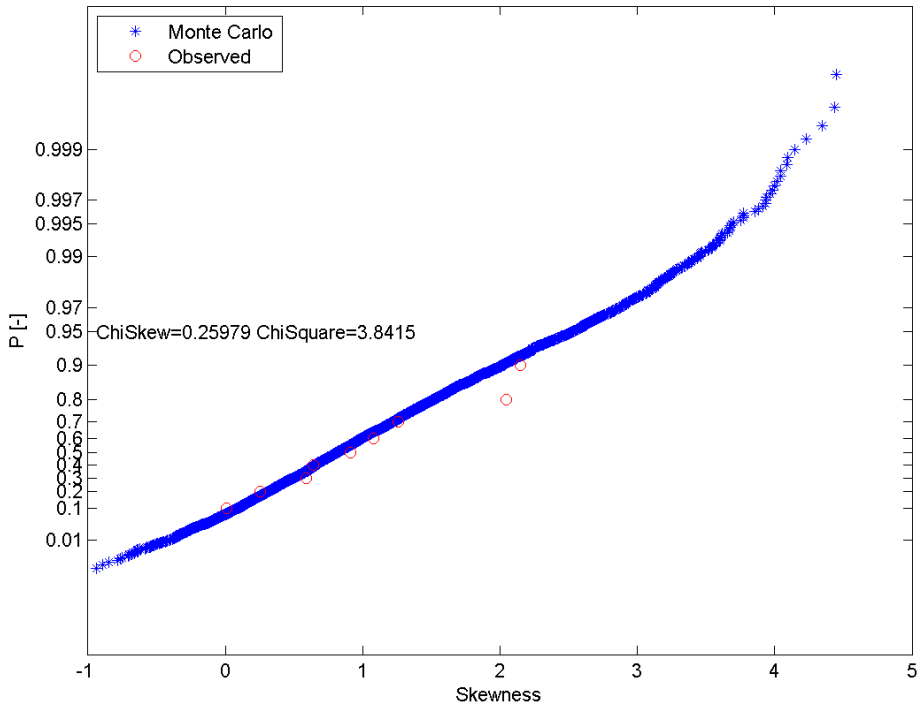

Figure 16 Example of homogeneity Chi Square test for the Skewness by means of Montecarlo technique. Gev distribution

Regression on the expected values:

Regarding the regression of the expected values we leveraged on previous analysis performed in the GAR 2011, using the same set of basin variables for the new analysis. Similar procedures have been followed (e.g., logarithmic transformation) to remove non linear dependences in the data.

For the variable selection a step-wise method have been used. Stepwise regression is a systematic method for adding and removing terms from a multilinear model based on their statistical significance in a regression. The method begins with an initial model and then compares the explanatory power of incrementally larger and smaller models. At each step, the p value of an F-statistic is computed to test models with and without a potential term. If a term is not currently in the model, the null hypothesis is that the term would have a zero coefficient if added to the model. If there is sufficient evidence to reject the null hypothesis, the term is added to the model. Conversely, if a term is currently in the model, the null hypothesis is that the term has a zero coefficient. If there is insufficient evidence to reject the null hypothesis, the term is removed from the model. The method proceeds as follows:

1) Fit the initial model.

2) If any terms not in the model have p-values less than an entrance tolerance (that is, if it is unlikely that they would have zero coefficient if added to the model), add the one with the smallest p value and repeat this step; otherwise, go to step 3.
3) If any terms in the model have p-values greater than an exit tolerance (that is, if it is unlikely that the hypothesis of a zero coefficient can be rejected), remove the one with the largest p value and go to step 2; otherwise, end.

Depending on the terms included in the initial model and the order in which terms are moved in and out, the method may build different models from the same set of potential terms. The method terminates when no single step improves the model. There is no guarantee, however, that a different initial model or a different sequence of steps will not lead to a better fit. In this sense, stepwise models are locally optimal, but may not be globally optimal, because of this reason the regression model have been fit both in an inclusive (from one to all) and exclusive (from all to one) way and the best result in terms of Correlation coefficient are retained. In most of the regions the "all possible regression" method have been applied and results compared with the ones of the stepwise method. Results were similar, due to the predominance of the Drainage area and mean rainfall as parameters dominating the regression in the majority of the hydrological homogeneous areas.

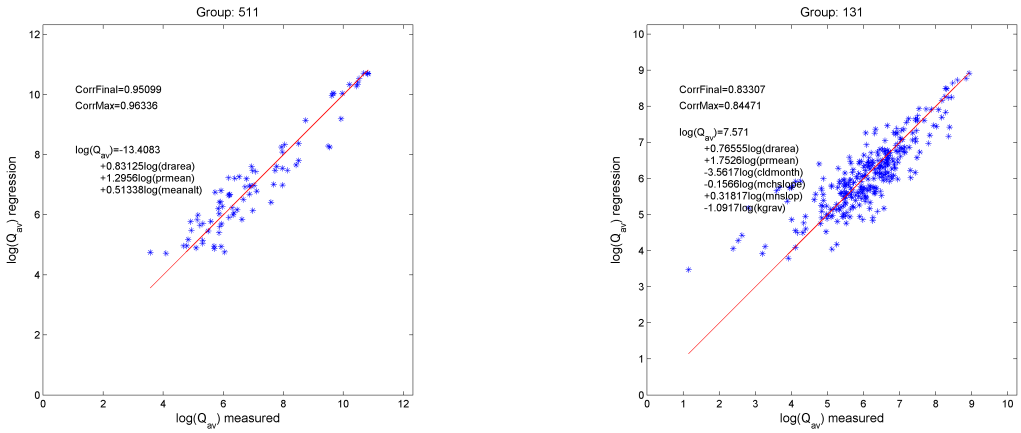

Figure 17 Regression for Index Flow estimation with basin variables; Group 511 (Asia) and 131 (North America)

Quantiles estimation

The final result of the procedure is the estimation of the quantiles associated to different return periods.

In the following the step by step procedure is reported.

The estimation of the regional growing factor is estimated with the following formulation that is valid for the GEV probability distribution.

$$X_T = \varepsilon + \frac{\alpha}{k} \cdot (1 - e^{-k \cdot yT})$$

Where:

$$yT = -\ln\left(\ln\left(\frac{T}{T-1}\right)\right)$$

With T=return period; ε, α and k are parameters valid for the homogeneous region.

The index flood is calculated for the single basin based on the main morpho-climatic characteristics of the catchment, using a formulation that is valid for the whole homogeneous area. It is derived by a regression carried out on the mean flow of the stations that belong to the area in the way described in section 0.

The estimation of the flood with a defined return period T is calculated with the following expression:

$$Q(T) = X_T \cdot e^{\ln(Q_I)}$$

The following figure shows the comparison of quantiles estimation using single site statistics, the regional distribution using the local mean for dimensionalizing the growth curve and finally the full regional approach using the regression for the index discharge estimation. We notice that the regional estimates provide normally a more consistent estimation with each other while in some cases the single site estimation can produce very different results especially for low frequency quantiles.

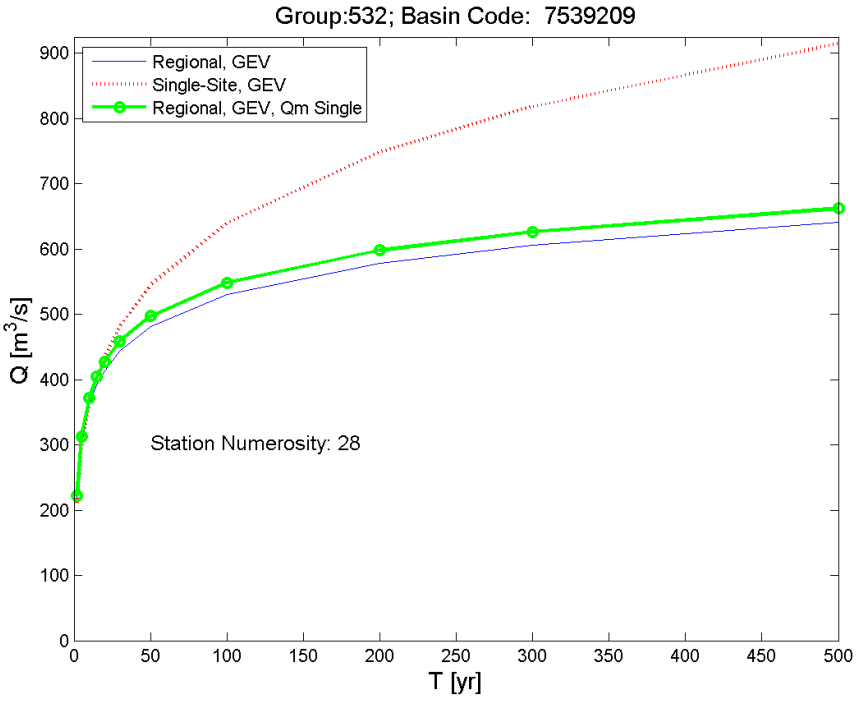

Figure 18 Quantiles estimation comparison using Regional and single site distributions; Group 532. The green line is the quantile estimation using Regional Approach regarding the growing factor while the Q_I is estimated as the average of the recorded flow data in the section.

Sections affected by dams

Another relevant issue is related to sections placed downstream a dam, or a system of dams. The presence of these hydraulic structures can influence the behaviour of the river in the downstream section even in high flow conditions, modifying the natural flow. During the floods the flood peak is potentially laminated by the artificial reservoirs.

A procedure to account for this effect has been implemented all over the world, starting from information available in the Global Reservoir and Dam (GRanD) database, updated March 2011. the Data base contains all major dams world round.

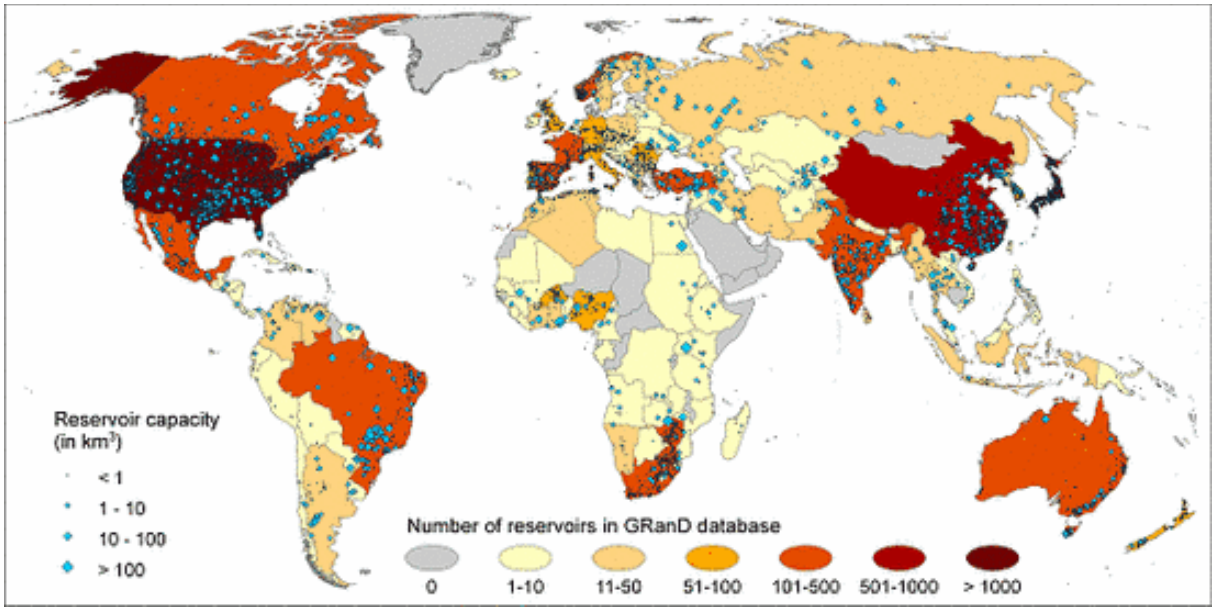

Figure 19 Distribution of dams in the GRanD Data Base

First the dams with a low lamination capacity have been filtered out. This has been done referring to the Degree of Regulation (DOR) field in the data base; equivalent to "residence time" of water in the reservoir; calculated as ratio between storage capacity and total annual flow. The total annual flow Long-term (1961-90) average discharge at reservoir location is derived from HydroSHEDS flow routing scheme combined with WaterGAP2 runoff estimates.

As a first approximation, we do not consider the dams that have a DOR<100%.

As a second step we identified those sections that we consider to be affected by the presence of one or more dams in the upstream basin

Let's consider the following quantities:

P_{ms}=mean of the monthly maximum precipitation for the section drainage area

A_s=drainage area of the basin upstream section

P_{md}=mean of the monthly maximum precipitation for the dam drainage area (equivalent dam)

A_d=drainage area of the basin upstream the dam (equivalent dam)

Compute the following metric:

$$WP_r = \frac{P_{md} \cdot A_d}{P_{ms} \cdot A_s}$$

WPr should generally be in the range (0-1).

We consider the section affected by the system of the dams upstream the section when WPr> TWP_r. TWP_r is fixed to the value 0.1.

In this way all sections potentially affected by the regulation capacity of the dam are marked. The third step is computing the laminated discharge quantile starting from the estimation given by the regional approach.

Basically we considered a synthetic event of rectangular shape of length 1 month and flow equal to the quantile estimation derived by the regional curve, this because we deal with monthly maximum flow. After that the percentage of flood volume that can be laminated by the dams is estimated with the following procedure.

1) Calculate the quantile with regional method in the analyzed section:

   $Q_{S,Reg}(T)=X(T)*Q_I$

   where X(T)= growing factor; Q_I=index flow

2) Estimate the percentage quantile flow due to the contribution of the basins upstream the dams:

   $Q_{UD,Reg}(T)= Q_{S,Reg}(T)*WP_r$

3) Estimate the quantile in the section masking the basins upstream the dams

   $Q_{SM,Reg}(T)= Q_{S,Reg}(T)*(1-WP_r)$

4) Estimate the maximum volume that can be laminated by the dam with an empirical function:

   $V_{D,MAX}$=K*Cap_max

   Where: Cap_max = 'maximum storage capacity' in cubic meters of the dams system derived by GRanD; K=min(0.25,Ks)

$$Ks = 0.1 + 0.15 \cdot \frac{(DOR - 100)}{200}$$

   K is thus a function of the DOR. The mean DOR of the system of dams upstream the section is considered.

The flow that cannot be laminated for the return period T is estimated as:

$$Q_{DD,\mathrm{Reg}}(T) = \max(Q_{UD,\mathrm{Reg}}(T) - \frac{V_{D,MAX}}{\Delta t};0)$$

Where Δt=30 days (converted in seconds); this because we consider max monthly flow and we refer to a synthetic event of rectangular shape with one month length.

Finally the estimation of the quantile in the section accounting dams' affection is calculated as:

$Q_{SF,Reg}(T) = Q_{SM,Reg}(T) + Q_{DD,Reg}(T) + Q_{Disch}$

Where:

Q_{Disch}= average discharge at reservoir location (the max value of the dams system is considered); this terms account for a base flow derived by the outlets of the dams and it is derived by GRanD.

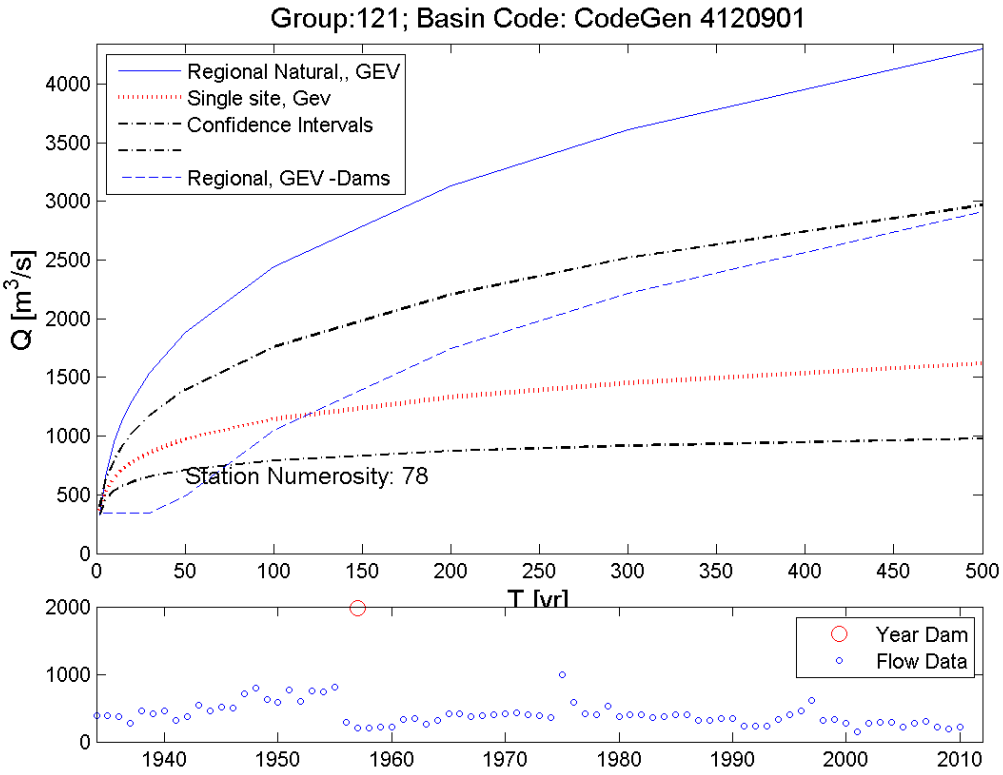

Figure 20 Example of quantile estimation for a section affected by the upstream dams. The blue continuous line is the regional estimation, the blue dotted line is the regional estimation accounting for the dams, the red line is the single site estimation while the black lines are the confidence intervals (90%) of single site estimation. In the low panel the monthly maximum flow data are reported together with the year of building of the dam (GRanD data).

Quantile estimation

Once the parameters of the growth factor and those of index flow formulation are defined the quantiles can be calculated for each section of interest. The section must be assigned to the right homogeneous region with the methodology described in paragraph 0.

To avoid inconsistencies in the case of rivers that cross more than one homogeneous region, a check on the quantile estimation has been introduced. When there is a passage from a region to another along the river bed from upstream to downstream the flow must always increase, otherwise the quantile estimation of the previous region is considered.

In Figure 21 an example of quantile estimation is shown, the final part of the rivers that flow in the gulf in front of Bangkok are considered.

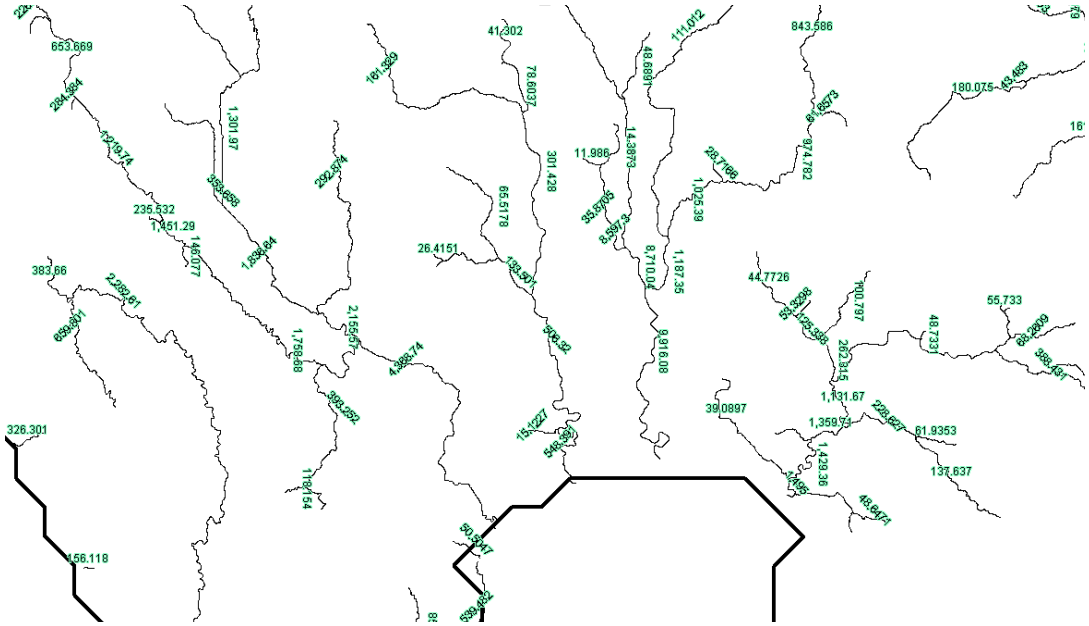

Figure 21 Quantiles estimation in the final part of the rivers that flow in the gulf in front of Bangkok.

Flooded areas Modeling

Once the discharge quantiles are determined, results are the input of a simplified hydraulic flood model. The current model stems from the one used in 2011 and further developed in 2013, and tries to improve its performance overall and in specific condition where the previous release model is recognized to have problems, mainly in flat and large flood plains as well as when river show a marked braiding.

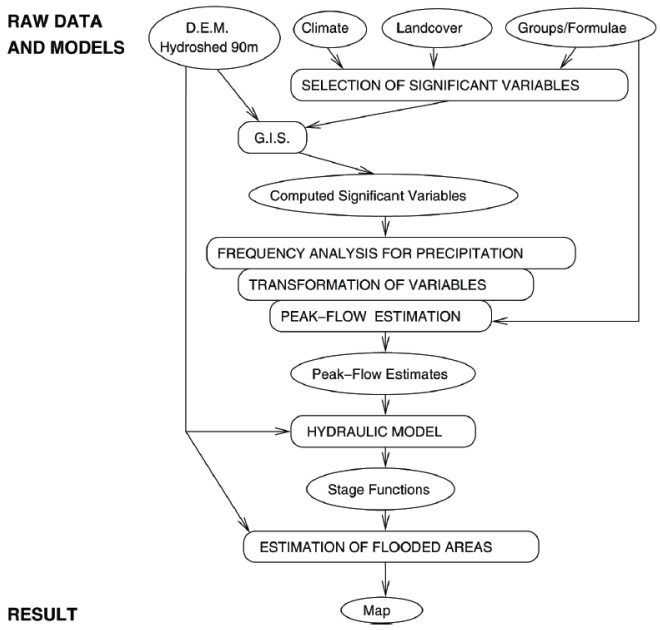

Figure 22 scheme illustrating the full workflow to obtain flood hazard maps for different return periods as per GAR 2011. The overall scheme can be considered valid for the current release.

The hydraulic model starts from an idea provided by the EROS Data Center (EROS/USGS). The original model first generates a relative DEM from HydroSHEDS that set any stream pixel values to 0 as a reference altitude. Then, it generates cross sections of a specified width for each stream section. Each cross section is then used to extract altitude values from relative DEM and generate a specific stage vs. discharge function using Manning's equation. These functions are finally used to calculate river stage from peak flow estimates for a specific recurrence interval, and then generate corresponding flooded areas for each stream section basin, using the generated relative DEM.

DEM improvements for hydraulic modelling

Hydrosheds is a hydrologically constrained DEM, so that the slopes identified by the DEM are suitable for depicting a hidrologically consistent drainage network. However, in the process of constraining the DEM to be respectful of a streamline system many artefacts arise. In particular streams are burned into the DTM creating fake canyons and deep gorges with unrealistic slopes in proximity of the real riverbed locations. This is preventing the DTM to be used as such for hydraulic computations and some pre-processing is needed to re-condition the DTM to more realistic elevations.

Here the reconditioning has been carried out recombining the Hydrosheds dataset, in the specific the drainage network that can be automatically extracted from the DEM, with the original point at 90m resolution derived from SRTM version 4.12 using a well known routine of interpolation specifically designed for the creation of hydrologically correct digital elevation models (DEMs) from comparatively small, but well selected elevation and stream coverages: the TOPODEM ArcInfo Command. It is based upon the ANUDEM program developed by Michael Hutchinson (1988, 1989). See Hutchinson and Dowling (1991) for an example of a

[2] http://www.cgiar-csi.org/data/srtm-90m-digital-elevation-database-v4-1

substantial application of ANUDEM and for additional associated references. A brief summary of ANUDEM and some applications is given in Hutchinson (1993).

The interpolation procedure has been designed to take advantage of the types of input data commonly available, and the known characteristics of elevation surfaces. This method uses an iterative finite difference interpolation technique. It is essentially a discretised thin plate spline technique (Wahba, 1990), where the roughness penalty has been modified to allow the fitted DEM to follow abrupt changes in terrain, such as streams and ridges.

Water is the primary erosive force determining the general shape of most landscapes. For this reason, most landscapes have many hilltops (local maximums) and few sinks (local minimums), resulting in a connected drainage pattern. TOPOGRID uses this knowledge about surfaces and imposes constraints on the interpolation process that result in connected drainage structure and correct representation of ridges and streams. This imposed drainage condition produces higher accuracy surfaces with less input data.

The global drainage condition also virtually eliminates any need for editing or post-processing to remove spurious sinks in the generated surface.

The drainage enforcement algorithm attempts to clear spurious sinks by modifying the DEM, by inferring drainage lines via the lowest saddle point in the drainage area surrounding each spurious sink.

This procedure has been applied on the entire Globe in order to produce an enhanced DEM dataset to be used for the simplified hydraulic flood model algorithm.

Model improvements

Some of the limitations of the original model have been removed. In its new version the model does not have the limit of having just one section per stream, which in certain cases could cause serious biases in the computation because of the length of the river steams. The new version of the model uses a sequence of cross sections per stream, whose density depends on the morphological characteristics of the catchment segment. In this way, it is possible to capture changes in the floodplain and in the cross section carrying capacity. In figure an example of such setup is showed.

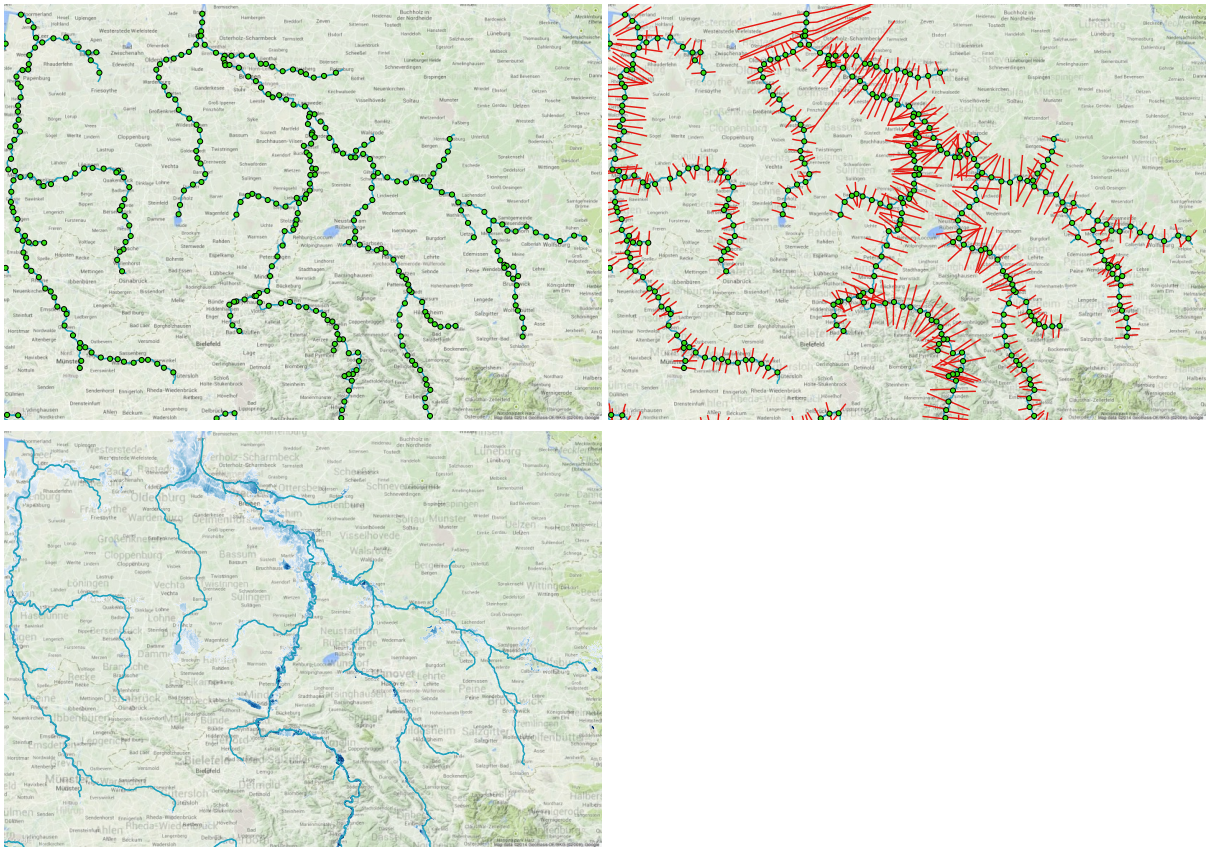

Figure 23 the schematic steps for the flood maps computation: quantiles computation at river sections; Rivers cross-sections delineation; manning equation application and water depths computation.

In the original model a single value of the Manning coefficient per stream was assumed, therefore making no distinction for long longitudinal river segments, and within the same cross section, making no distinction between riverbed and flood plain hydraulic roughness. Such an approximation is a critical one as the Manning coefficient is the main parameter to determine the discharge stage transformation. This limitation has been removed and the manning parameter cannot only change between cross sections along the streams, but within the cross section itself where normally the main channel and the floodplain show very different hydraulic roughness. In the model new version flow in the floodplain is subdivided as the roughness coefficient changes along the cross section. The Manning equation in terms of conveyance is used. For the conveyance computation the cross section is subdivided into segments with limited differences in flow velocity that is determined by the hydraulic roughness. All the incremental conveyances are summed up to obtain a conveyance on the floodplains and in the main channels that ultimately determine the total conveyance of the cross sections and therefore the stage discharge curve.

The Manning coefficient is determined for the different parts of the cross section on the basis of the land use map provided by the Glob Cover map.

A second important modification regards the possibility of determining stage discharge curves in braided rivers that for certain flow conditions present transversal hydraulic disconnections in the cross section. This condition has to be accepted in case of braided rivers and disregarded in other cases arising from specific morphologic conditions. Therefore

on the basis of discharge value and slope value a likelihood of the river being braided is determined and a possible extension of the flood plain where hydraulic disconnection is allowed computed on the basis of a simplified steady flow computation based on a regularized triangular representation of the cross section.

In the flood plain especially were the morphological control is low (i.e. flat areas) the concept of relative DEM as a boundary for the flood plain fails. Such limitation is overcome by iteratively recomputed the cross section so that the manning equation is satisfied imposing that as a limit for the flooded area. The cross section points are then connected following the local slope value.

Another evident limitation of the model was the impossibility of representing the backwater effect occurring in certain areas of the globe. It is possible in fact that a flooding plain pertaining to a tributary is not flooded because of the limited carrying capacity of the tributary itself but because of the valley boundary condition imposed by the main river that blocks the discharge from the tributary diminishing its capacity, and imposes a higher free surface level in the valley par of the tributary. This has a large impact in flood extension computation when the tributary slope is really low. This case has also been solved in the new version. Junctions where a minor tributary showing a limited slope and a major river (with a quantile discharge more than one order of magnitude tributary) intersect are identified. In this case the water height imposed by the main river is propagated backward along the tributary with a rate of decrease that takes slope into account till the height imposed by local calculations on the tributary does not exceed such value.

Observed flood events

In addition to modelled floods, nine years of actual flood events, as detected by satellite from Dartmouth Flood Observatory (DFO[3]), were incorporated. The observed flooding events, based mostly on MODIS satellite sensors at 250 m resolution, provided additional information and were also used for calibration. The data for observed flood events cover only nine years, containing more than 400 events and are not comprehensive. In addition to the DFO Database the UNOSAT Flood Portal[4] had been used extensively for validation. The portal enables access to 20 years of activations from UNOSAT and all products are downloadable in various formats. The flood footprints here are derived from different sensors (optical and SAR) and at different resolutions (from Medium resolution to Very High Resolution).

Taking into account flood defences

The methodology presented so far is able to identify floodable areas without considering the impact of flood defenses that are commonly put in place to defend high concentration of values (e.g. urban areas). While for high return periods (i.e. 200 years and above) the assumption of flood defenses partial of total failure is an acceptable hypothesis that is often used also in local risk assessment studies, this hypothesis cannot be supported for the more frequent floods (i.e. 100 years return periods or lower). To neglect the flooded volume and

[3] http://floodobservatory.colorado.edu
[4] http://floods.unosat.org/

extension in this second case would lead to a certain overestimation, especially in developed Countries that invested since distant times in river regulation and flood defenses.

However, taking into account flood defenses is one of the biggest hurdles when dealing with catastrophe models especially on large domains. This is especially true when acting at global scale, where the scale of the model does not allow to automatically representing flood defenses and where no layer indicating flood defenses position is available.

It is therefore needed to implement an approximated methodology based on sensible hypotheses.

It is reasonable to hypothesize that investment in flood defences are a function of the values to be defended both in economic and human terms. The GDP distribution could represent both the economic interest concentration and can be considered as a proxy of human activities, and it is considered at this stage as the best possible proxy available at global level. Figure 24 shows the idea behind the defence algorithm. The y-axis reports the defence level measured in term of target return period as a function of the GDP in a given area. The curve assumes that we need to reach a certain threshold in terms of GDP concentration in order to start worrying about flood defences (X1), after that investment in flood defences increases with GDP, after a second threshold (X2) the investments slow down till threshold X3. From there the inclination to invest in flood defences rises up quickly again and reaches a high level (T4), this is the case of big urban centres that concentrates high GDP values as well high people concentration. T4 depends on the investment capabilities of each Country.

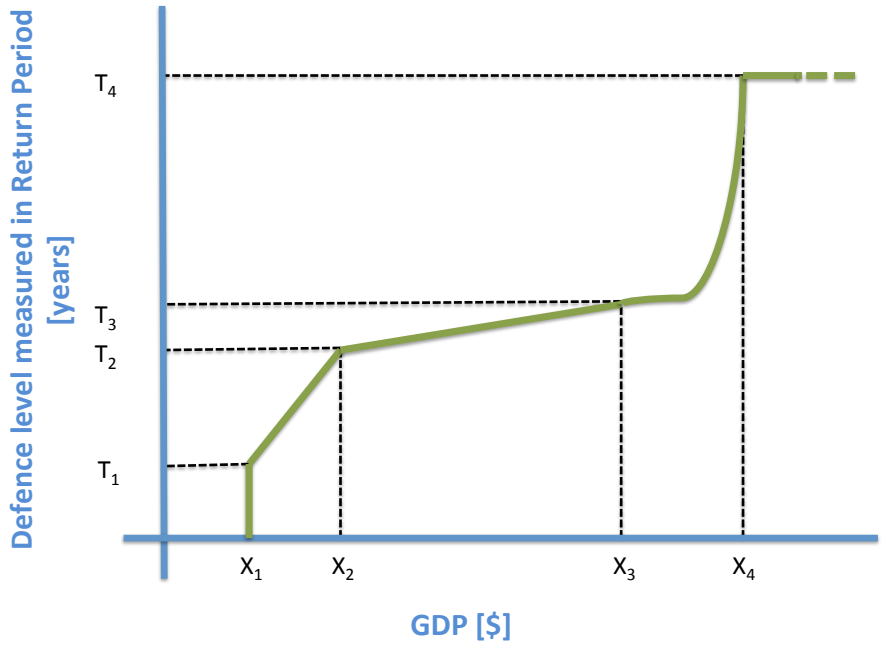

Figure 24 inclination in investing in flood defences as a function of GDP

Along these lines the following algorithm has been designed.

The algorithm starts from the GDP map, a rasterized river network map where each stream has a unique value for all its pixels and the 100 years return period flood hazard map

The first step of the algorithm isolates the pixels that concentrate more than a threshold GDP in Log10 scale. The threshold value is chosen to properly isolate the urban centres. On the filtered layer the centroids of all connected areas of non-null GDP are identified, only the ones falling into the 100 years return period are retained. Successively an area of respect (i.e. the area to be defended) is computed for each centroid. The area of respect computation develops along the following steps (refer to Figure 25 for the symbols):

a. Compute the diameter d_c of the connected area corresponding to the centroid (minimum value: $2dx$ with dx spatial resolution of the raster)
b. Identify the stream s nearest to the centroid
c. Compute the distance d_s between the centroid and the nearest pixel P of the stream s
d. Construct an ellipse oriented in order to have one axis passing for the centroid and the point P (this is often the major semi-axis, but not always). In this direction the semi-axis is long $1.1d_s$ while the other semi-axis is long d_c
e. Find the maximum value GDP_{MAX} of the GDP inside the connected area
f. Compute the Defended Return Period T_{RD} as $T_{RD}=T_{RDmin}+(T_{RDmax}-T_{RDmin})*[(GDP_{MAX}- GDP_0)/(GDP_{MAX}- GDP_0)]^4$. This is the value that is attributed to the ellipse, that represents the Defended Area relative to the given centroid.

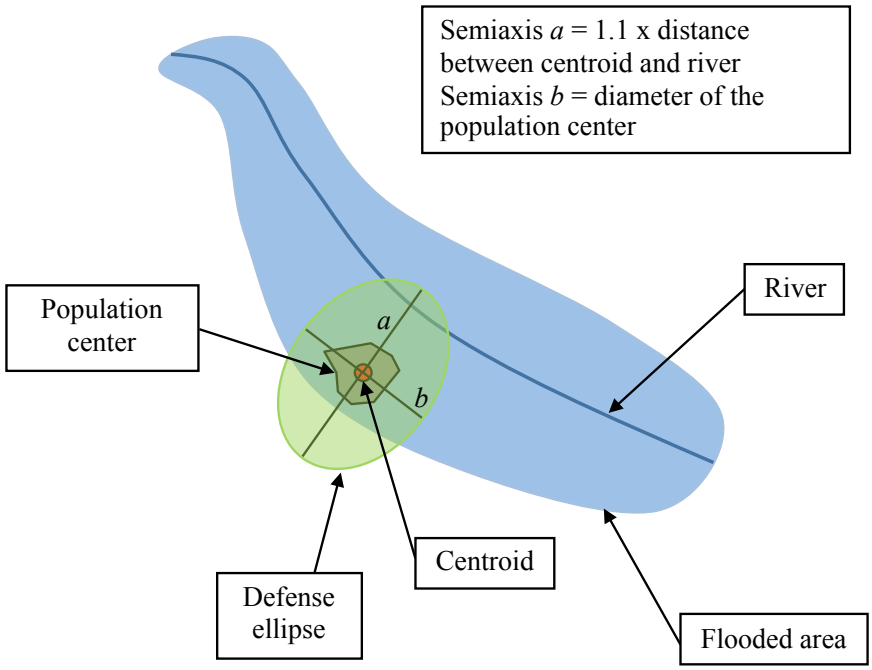

Figure 25 illustration of the area of respect computation.

Flood defences are assumed not to fail till the design RT of the defences is met. After that Overtopping occurs. With increasing Return periods, partial defence failure is considered. As an example, a 200-year defence would partially fail for a 500-year event (e.g. for a partial levee breach) and would fail even more for a 1000-year event, this on top of the "overtopping" of the defences that will any case occur. The defences are functional till the their design return period, therefore the protected site will not experience any loss till that the intensity is reached.

Hazard maps examples

In this paragraph some examples of hazard maps are compared with satellite retrieved flood footprints for the Thailand flood 2011/2012.

This comparison is meant to test the overall capacity of the Hazard maps in identifying the flooded areas when analysed at full resolution. It is generally expected that the observed (i.e. satellite derived) flood area is lower than the simulated one, due mainly to the non-contemporaneity between the flood event and the satellite acquisition. In the case of Thailand however the water residence time was long enough to minimise the above mentioned problem.

Severe flooding occurred during the 2011 monsoon season in Thailand. Beginning at the end of July triggered by the landfall of Tropical Storm Nock-ten, flooding soon spread through the provinces of Northern, Northeastern and Central Thailand along the Mekong and Chao Phraya river basins. In October floodwaters reached the mouth of the Chao Phraya and inundated parts of the capital city of Bangkok. Flooding persisted in some areas until mid-January 2012, and resulted in a total of 815 deaths (with 3 missing) and 13.6 million people affected. Sixty-five of Thailand's 77 provinces were declared flood disaster zones, and over 20,000 square kilometres of farmland was damaged[5]. The disaster has been described as "the worst flooding yet in terms of the amount of water and people affected."

The World Bank has estimated 1,425 billion baht (US$ 45.7 Bn) in economic damages and losses due to flooding, as of 1 December 2011[6]. Most of this was to the manufacturing industry, as seven major industrial estates were inundated by as much 3 meters (10 feet) during the floods. Disruptions to manufacturing supply chains affected regional automobile production and caused a global shortage of hard disk drives, which lasted throughout 2012.

The new version of the GFM was therefore run for the Thailand area so to have a fresh comparison of the result with this catastrophic event. Figure 26 depicts the flood maps for Thailand for three different return periods (T = 25, 100, 200 years). There are differences between the three maps both in flooding extension and water depth values. The biggest differences concentrate in the Bankog area, due to the defences that are mimicked in the maps. For the rest the small differences are due to the climatic specificity of the area.

[5] "□□□□□□ □□□□□□□□□□□□□ □□□□□□□ □□□□□□ □□□□□□□□□□□□□ □□□□□□□ 129 □□□□□□ 17 □□□□□□ 2555 (Flood, storm and landslide situation report)" (in Thai). 24/7 Emergency Operation Center for Flood, Storm and Landslide. http://disaster.go.th/dpm/flood/news/news_thai/EOCReport17JAN.pdf

[6] http://www.worldbank.org/en/news/2011/12/13/world-bank-supports-thailands-post-floods-recovery-effort

Tropical catchments show in fact small differences between quantiles (small variance in the quantiles) that leads to a very steep growth curve. This in combination with the methodology used to derive the maps results into relatively small differences in flood extensions. However local differences might be striking. Figure 26 also shows a comparison between the GFM results (25 years return period) and the DFO footprint. The match is very good especially in mountain areas where the morphologic control is dominant and the GFM methodology more reliable.

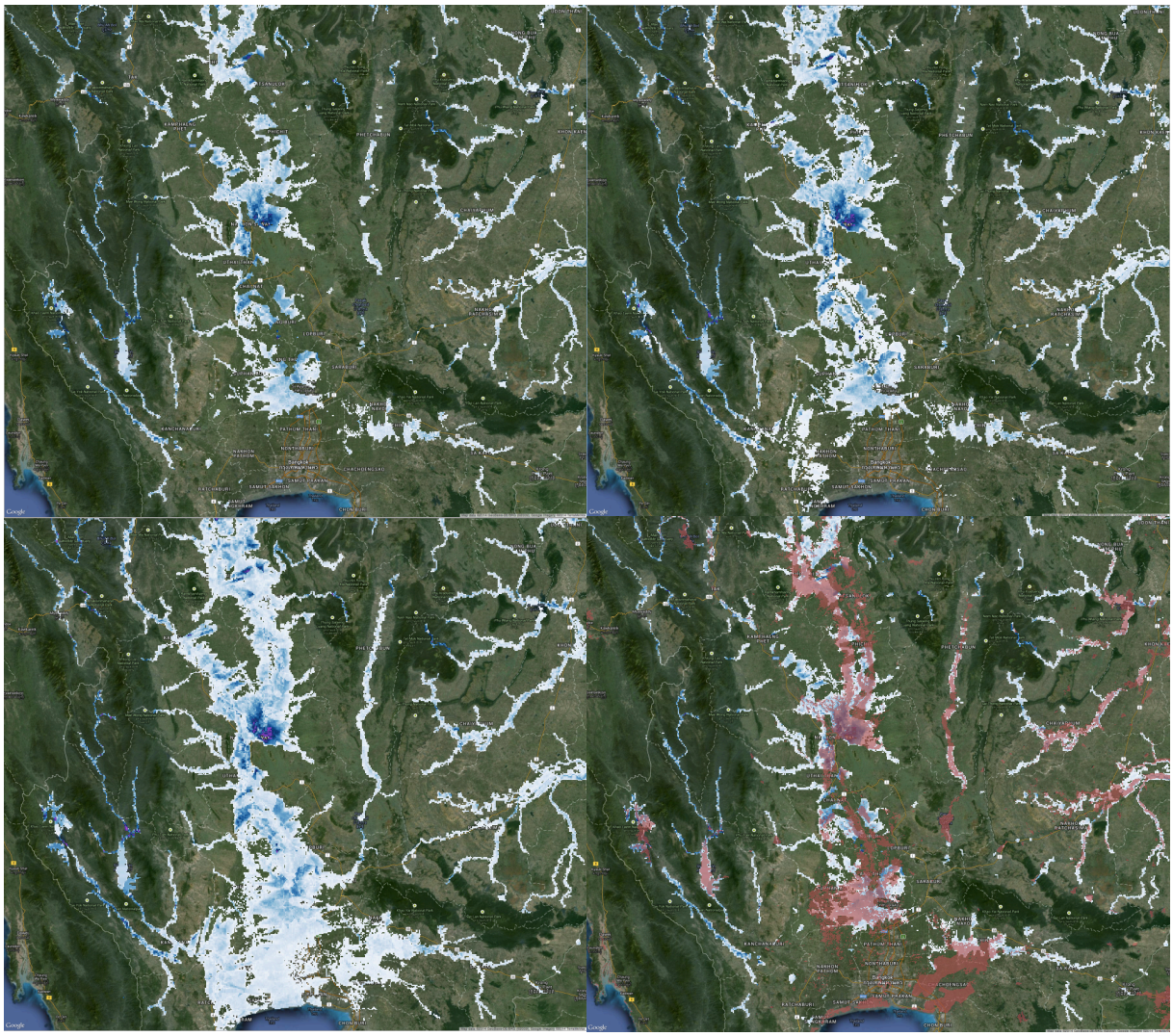

Figure 26 Flood maps for Thailand for three different return periods (from left to right from top to bottom: T = 25, 200, 1000 years) and bottom right panel DFO flood footprint envelope layered on the flood map for T = 100 years. Reconditioned DEM in the background.

A more detailed comparison has been possible in this case thanks to some Hi-RES flooded areas provided by UNOSAT based on a combination of Hi-Res SAR and optical images.

Figure 27 presents the comparison and shows the multi temporal envelope of flooded areas from the beginning to the end of the flood event 2011. The limits are followed quite well by the GFM predictions it is easy to see how the defences in the Bankog area play again an important role improving the match between the hazard maps and the satellite retrieved maps.

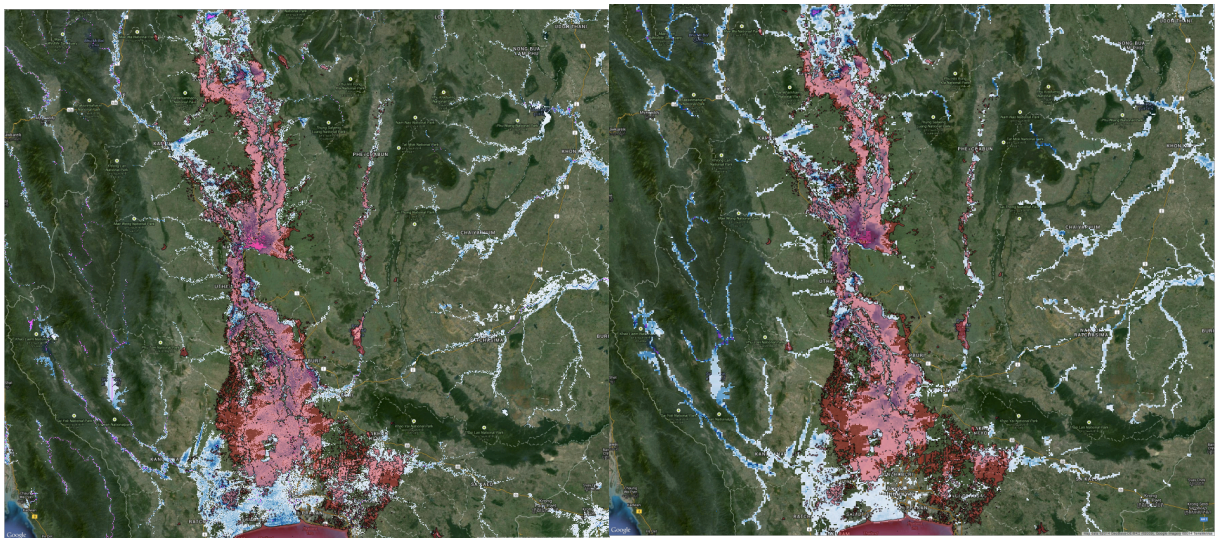

Figure 27 Flood maps for Thailand for two 200 years return period undefended (left panel) and defended (right panel compared with the UNOSAT flood footprint envelope of 2011 event.

Model validation - Hazard

When looked at country scale the Hazard maps sequence often fails to highlight the differences amongst the 6 reference return periods used as a basis for the risk computations. In order to discuss better such differences in quantitative terms Figure 28, Figure 29, Figure 30, present three panels reporting the frequency histogram of water depths for the 6 return periods respectively for Colombia, Germany and Thailand.

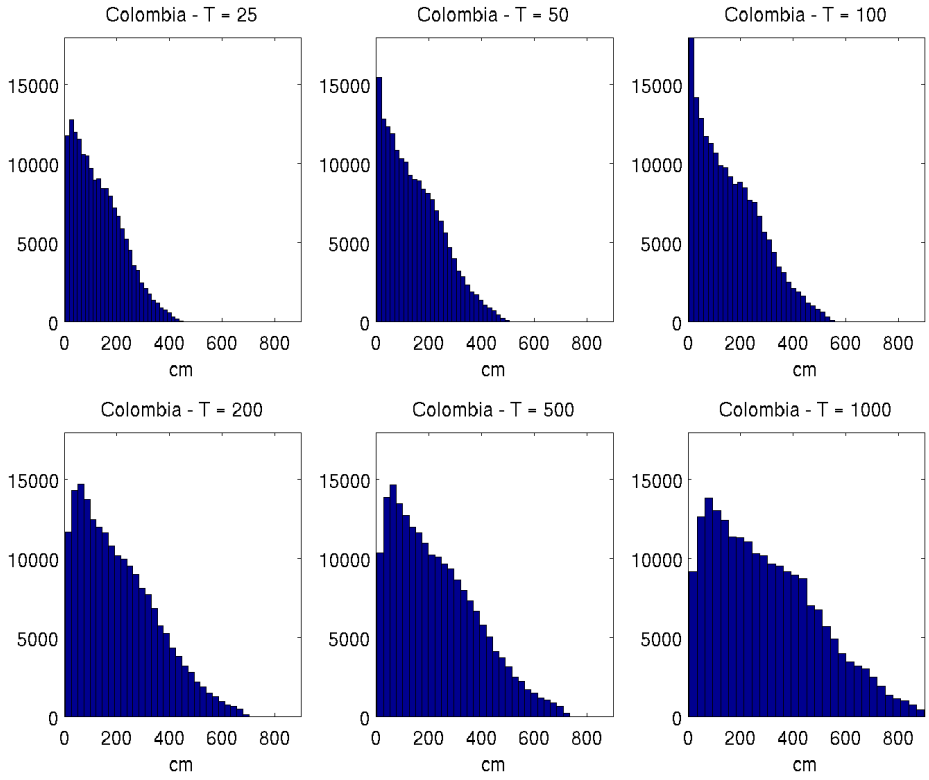

Figure 28 COLOMBIA: histogram of Water Depths for the 6 return periods

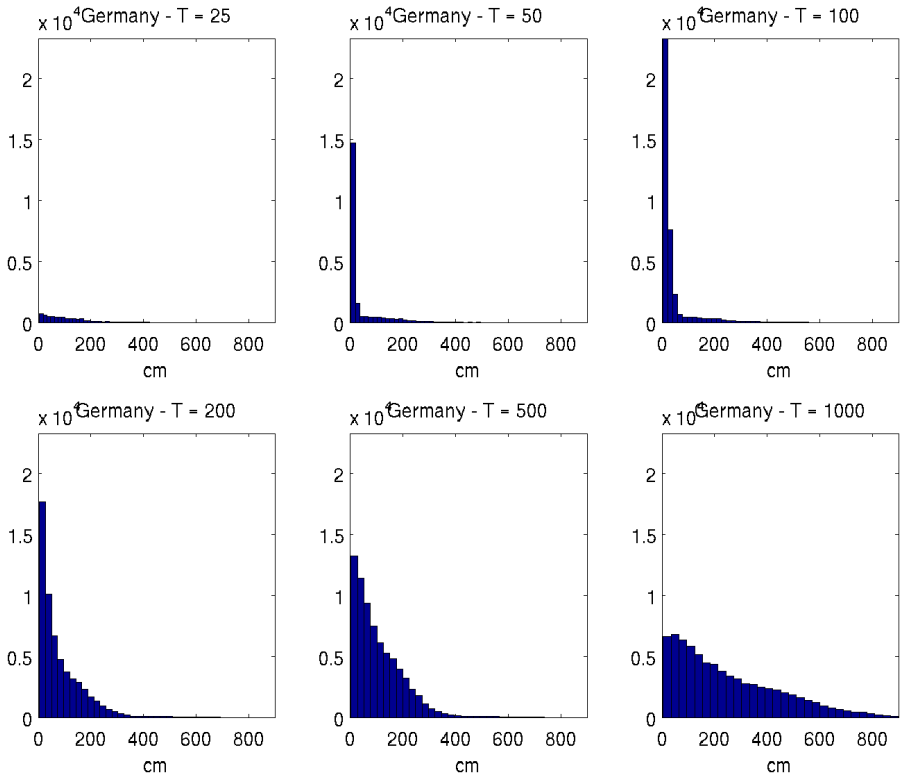

Figure 29 GERMANY: histogram of Water Depths for the 6 return periods

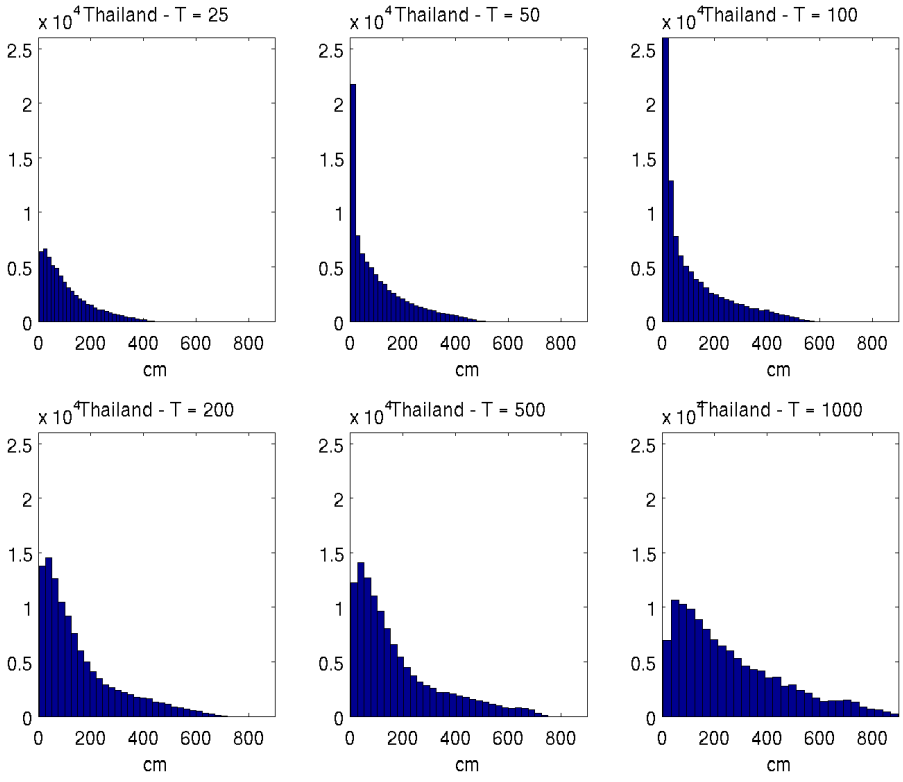

Figure 30 THAILAND: histogram of Water Depths for the 6 return periods

In the case of Colombia, the 25 return period presents already a relatively fat tail towards the high water depth values, although its mode is very close to few centimeters of modeled water depth. Such a behavior is not normally to be expected and has been better investigated. In the map several high values (higher than 5 meters) can be spotted, concentrated in very specific geographical areas. Two main reasons can be ascribed to this behavior of the model. The first, and more impacting one, is because of the values that the DTM assumes in some areas that are often covered with water (e.g. marsh-lands or lakes' expansion areas). The SRTM DEM is derived form the backscatter signal form SAR data. This signal is strongly affected by water that is a highly reflecting surface and in those areas the DTM presents many times inaccurate values. Automatic pit filling procedures are often not effective in correcting or reducing such errors. This should have a minor impact on risk calculation as it is expected that little exposure concentrates in these areas. However, in the process of aggregation from 90 meters (native model resolution) to 1 km and its successive merge with a 5 km resolution exposure might create overestimation of risk close to these areas.

Figure 31 depicts an example of such situation in northwestern Colombia.

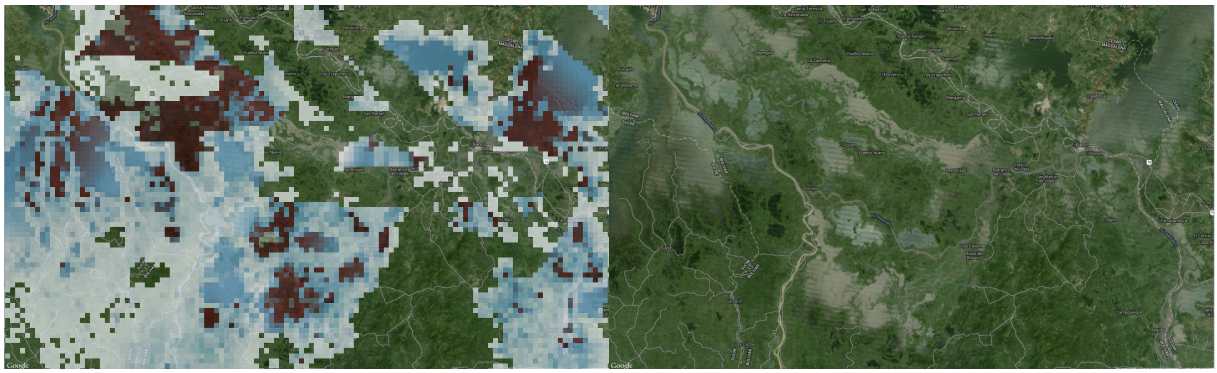

Figure 31 Water depths higher than 5 m are shown in the first panel in red, the second panel shows the satellite image of the area: permanent water bodies are clearly distinguishable.

The second reason is much less impacting though diffused in the map. In some places the valley morphology is really narrow so that one single pixel covers the whole valley at 1 km resolution. Therefore during the aggregation process some river pixels are included in the value computation biasing the pixel value (Figure 32).

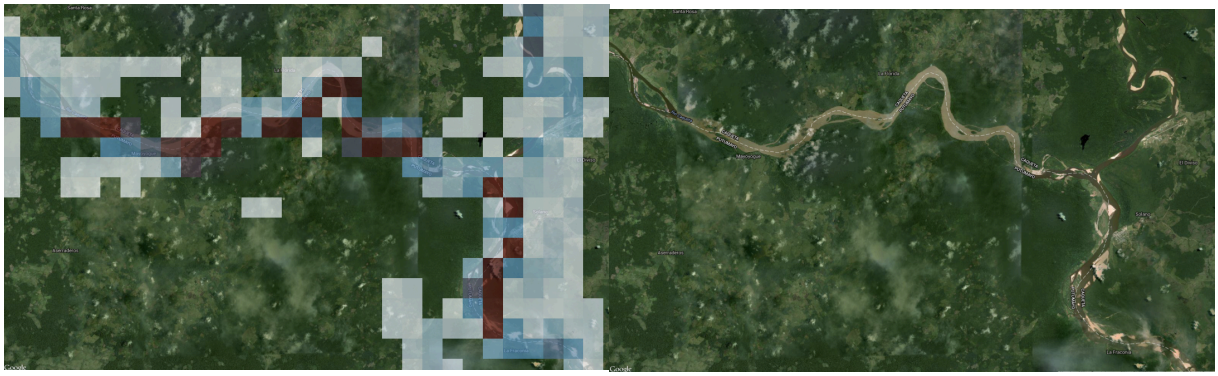

Figure 32 Water depths higher than 5 m are shown in the first panel in red, the second panel shows the satellite image of the area: permanent the riverbed is clearly distinguishable.

The histogram tend to shift the mode value and to increase the frequency values with increasing return periods as expected. After 200 years return period the mode is not any more close to zero and moves to from about 1 meter for 200 years to more than 1.5 meters for 1000 years. The tails also tend to become more and more fat in for high water depth values.

Panels for Thailand and Germany show a much more regular behavior. They show a very peaked histogram for low return periods where almost all values are concentrated in a very narrow band of water depth values and the mode is very close to 0 values. With increasing return period the tail grows, the median remains located close to 0 while the mean water depth value increases slowly till 100 years. From 200 to 1000 years the mode departs from 0 and the overall distribution shows higher frequencies in the distribution's tail as expected.

The issue of scale

Some further considerations are due with regards to the scale used for the hazard maps computation and the one successively used for the risk computation. The native resolution of the hazard model is 90 m, the resolution of the STRM GDEM. This resolution seems to be good for capturing the main features of the flood process for large rivers that are the main focus of this work. For reasons linked to the scale of the available exposure data an aggregation of the hazard results have been necessary at the 1 km scale. The hazard maps have been resampled at 1 km by reporting in the larger pixel the median of the values of the 90 m pixels. The median has been preferred to the mean value as it is less influenced by tail values (i.e. too low or too high values). A river mask has been produced on the basis of the hydraulic modeling and such mask is applied during the median operation so that high values in the river are not affecting the aggregation in pixel that intersect the river segments (see e.g. Figure 33).

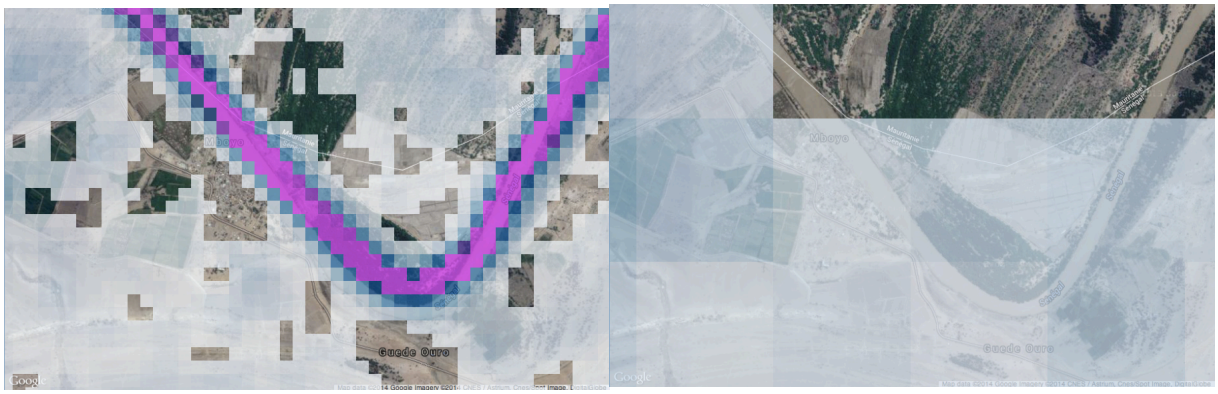

Figure 33 the left panel shows the 25-year map for Senegal at 90 m resolution (river mask is in magenta), on the right hand panel the same map at 1 KM resolution, in this case the water mask worked properly in filtering out the high values in the river (consider that the right side of the river is in Mauritania and it is not considered in the 1km map that is cookie cut on the Country border)

However, such mask is an approximation and it is in many cases not sufficient to remove the problem completely, however it has been verified that such problem is limited to special cases. In Figure 34 one of these cases is shown. In the 90 m map the small village in on the left side of the Senegal River is spared by the 25-year flood extension and all water depth values in the surroundings are less than 50 cm. When aggregated at 1 km scale the two pixels in the center of the figure include some pixels in the river bed that are not filtered out

by the water masks as a result we have an assigned water depth of such pixels to 3.5 m. In addition the resolution is such that the village is now interested by the flood extension with a high water depth value. This second issue is even more impacting as the extension of the 1km map are on average significantly larger than the one at 90 m. This can be easily seen in Figure 35 that presents a comparison of the 25-year return period for Senegal at the 2 scales at two zoom levels.

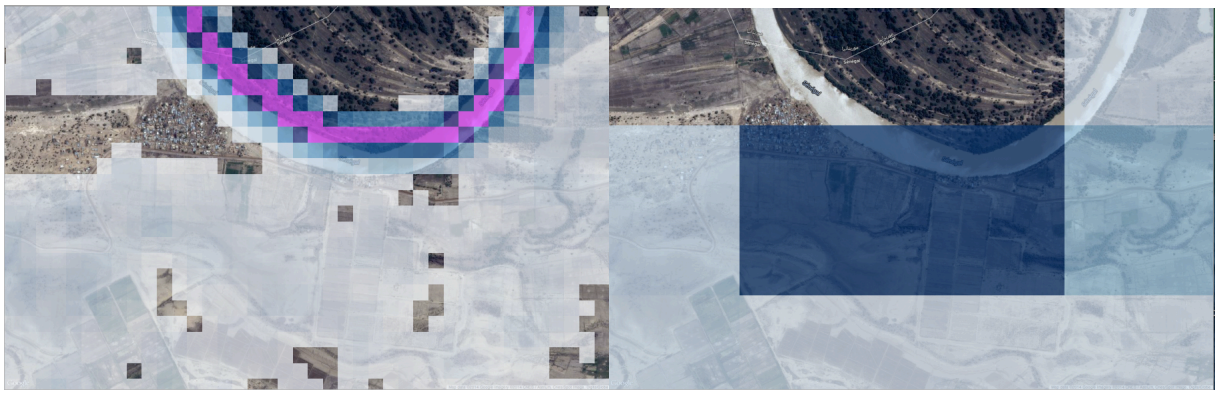

Figure 34 the left panel shows the 25-year map for Senegal at 90 m resolution (river mask is in magenta), on the right hand panel the same map at 1 KM resolution, in this case the water mask worked properly in filtering out the high values in the river (consider that the right side of the river is in Mauritania and it is not considered in the 1km map that is cookie-cut on the Country border)

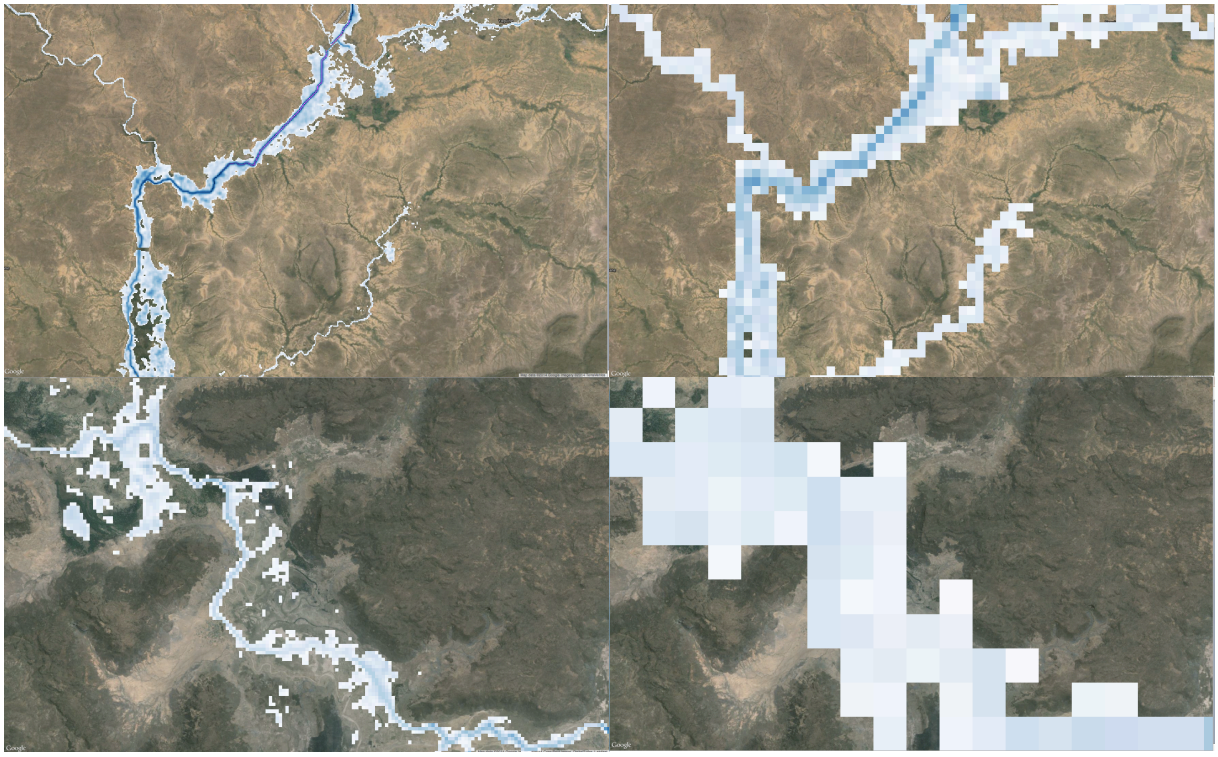

Figure 35 the upper left panel shows the 25-year map for Senegal at 90 m resolution, on the upper right hand panel the same map at 1 km resolution, the lower panels show the same information for a detail. It is evident the effect of aggregation in enhancing the hazard map overall extension.

Domain Considered	% of inundated area in the domain at 90 m resolution	% of inundated area in the domain at 1 km resolution	Ratio Inundated Area 1 km /Inundated area at 90 m
AF_1	0.83	4.36	5.24
AF_10	2.32	5.06	2.18
AF_11	1.53	4.94	3.24
AF_2	0.88	5	5.71
AF_3	1.27	5.22	4.1
AF_4	1.73	4.9	2.83
AF_5	1.89	6.68	3.54
AF_6	2.32	5.01	2.16
AF_7	2.35	6.67	2.84
AF_8	1.45	3.69	2.54
AF_9	1.09	3.69	3.4
AU_1	2.5	5.25	2.1
AU_2	1.12	3.38	3.01
AU_3	2.76	5.53	2.01
AU_4	0.42	1.15	2.75
EA_1	4.84	9.04	1.87
EA_10	0.94	5.08	5.38
EA_11	2.6	6.03	2.31
EA_12	3.02	6.58	2.18
EA_13	1.1	3.54	3.21
EA_14	4.42	8.25	1.86
EA_15	2.02	4.37	2.16
EA_16	0.97	2.48	2.56
EA_17	0.44	1	2.26
EA_18	0.74	2.2	2.96
EA_19	0.1	0.26	2.65
EA_2	2.43	4.49	1.85
EA_20	0.08	0.19	2.42
EA_21	1.5	3.38	2.26
EA_22	3.06	6.12	2
EA_3	3.34	6.08	1.82
EA_4	1.15	3.36	2.91
EA_5	1.5	4.03	2.69
EA_6	2.54	5.08	2
EA_7	2.65	5.86	2.21
EA_8	2.59	5.12	1.98
EA_9	1.17	3.21	2.74
NA_1	1.06	2.68	2.53
NA_2	3.79	6.95	1.83
NA_3	4.75	8.13	1.71
NA_4	0.99	3.03	3.07
NA_5	2.37	5.56	2.34
NA_6	1.53	3.43	2.23
NA_7	0.89	2.07	2.32
NA_8	0.26	0.56	2.15
SA_1	2.29	5.61	2.44
SA_2	0.62	1.47	2.38
SA_3	3.8	10.73	2.83
SA_4	1.58	4.02	2.55
SA_5	0.59	1.57	2.65
SA_6	4.81	8.61	1.79

Table 1 Inundated areas statistics for different resolution of the Hazard maps for 1 of the reference return period.

Model validation - Risk

The Global Flood Model has been extensively validated on the basis of available information: e.g. through satellite footprints form different sources, hazard maps at country level when available, analysis of the Frequency distribution of the hazard levels. The limitations of the

methodology and their reflection in the results have been already discussed in previous sections.

It is difficult to validate risk results in an exhaustive way as the GAR results in terms of risk economic figures are not available for other sources at the time this paper is written. It is therefore necessary to compare with different benchmarks where possible in order to increase the reliability of the results.

The AAL results obtained from the flood models have been compared with:

- Historical loss data derived AAL estimations from the Desinventar initiative where the loss database was long enough to render a reasonable estimate of the AAL range.
- Other historical loss estimation available at Country level
- For Europe a sanity check was done against the solidarity fund statistics
- With expert judgment from expert and professionals working in catastrophe modeling
- With estimates derived from other global models showing comparable statistics
- Through cross comparison with the AAL obtained from other hazard in the context of GAR

The following table summarizes the overall results for some benchmark countries:

			HAZARD from GAR		ACQUADUCT [assuming 15 years defence]	ACQUADUCT [defence level needed to reach similar results to GAR]
Country name	Region	Exposed Value (from GED) [USD Million]	AAL [USD Million]	AAL [‰]	AAL [USD Million]	T [years]
Bangladesh	Asia	$381,431.88	$2,463.17	6.46	$3,950.00	27
Bosnia and Herzegovina	Europe	$30,656.21	$54.71	1.78	$313.18	90
Colombia	Latin America and the Caribbean	$859,720.00	$654.81	0.69	$833.90	20
Germany	Europe	$15,114,873.00	$2,697.57	0.18	$15,510.00	100
United Kingdom	Europe	$7,806,797.00	$870.03	0.11	$4,710.00	90
Guatemala	Latin America and the Caribbean	$168,700.00	$68.73	0.40	$138.52	30
Japan	Asia	$39,255,204.00	$4,328.00	0.11	$15,040.00	60
Cambodia	Asia	$27,390.49	$251.19	9.17	$277.06	16
Mozambique	Africa	$36,409.45	$39.00	1.07	$64.34	26
Romania	Europe	$555,697.44	$519.75	0.94	$1,140.00	35
Chad	Africa	$26,745.14	$38.75	1.45	$90.30	40
Thailand	Asia	$1,378,998.63	$2,586.19	1.88	$5,720.00	40
Vietnam	Asia	$487,574.38	$2,295.39	4.71	$4,180.00	30

Figure 36 summary of the risk computations per countries compared with the Deltares model from the acquaduct Project.

Estimates show AAL values that rank from less than 1 per mill in countries where it is expected that a big investment in flood defences has been made (e.g. UK and Germany) to 1 per cent in countries where less investment has been made and their particular climatic and morphologic situation enhances the risk of extended floods. Inter-comparison between vulnerability libraries evidences a reduction of the AAL when modified curves from CAPRA of from GA were used (see general BG paper on risk computations for details). The original curves in CAPRA were most fit to represent low quality settlements and they have been

modified in order to better represent non-informal settlements in developed countries. That is the reason why the effect of changing the curves is particularly evident in developed countries where the quality of the built up environment is expected to be higher. The table shows also a comparison with the Aqueduct project[7] that enables to calculated the GDP portion interested by a flood with assigned return period. The Project web interface allows also placing a uniform defence level in the country expressed in terms of Return Period. The table reports the AAL values with at uniform 15-year defence all over the countries and in another column the level of defence needed to reach comparable results with the GAR GFM. As expected the results from Acqueduct are normally higher, but the order of magnitude of the results is comparable.

Implementation of a hydrologic model for stream flow simulations worldwide

As discussed in the executive summary the aim of the GAR 2015 flood model was also to test changes in a Climate Change environment. In order to do that to rely only on streamflow data is not obviously possible and a proper reconstruction of possible streamflow time series has to be performed.

In order to do that it is necessary to set up a proper modelling chain that has at its heart a hydrologic model able to capture the underlying processes determining flood condition changes. The application of an hydrologic model, necessary to fulfil this part of the work has several advantages on other parts of the work too. Specifically, the possibility of reproducing stream-flow time series even in present climate can be used to validate or improved the regionalization results especially in places where the observations are lacking. Secondly, full-scale stream-flow simulations deliver crucial information for the single flood scenarios creation, scenarios to be used for the full probabilistic assessment for the derivation of the PML curves. This last point is still under validation and will not be discussed in detail in this background paper.

Nowadays many hydrological models are made available to the scientific and research Community even in open source fashion and it is sometimes hard to decide for the best tool to be used.

In the case of this application, there are however features needed that can shorten the list of the candidate models. The model needs to be a Continuous Hydrologic model with a proper description of all key hydrological processes including a proper energy budget solver. This is needed in order to capture properly the initial condition sequence that in the case of many climate environments worldwide plays a key role in determining the flood events.

For these reasons and for the familiarity that the research group has with the model the Continuum model (Silvestro et al., 2013) has been selected. The model is a compromise between models with a strong empirical connotation, which are easy to implement but far from reality, and complex physically based models which try to reproduce the hydrological

[7] http://www.wri.org/our-work/project/aqueduct

processes with high detail but which introduce a hard parameterization and consequent uncertainty and lack of robust parameters identification.

The Continuum model aims at an equilibrium between simplicity and rigorous physical modeling while maintaining comparable performances to existing models; the reduced complexity of the schematizations and the relatively small number of parameters leads to a considerably lower calibration effort, increasing model robustness and portability to data scarce environments. The resulting increased computational efficiency leads to an easier utilization of the model in ensemble mode so that a direct quantification of prediction uncertainties is possible, or in this this case it eased the computational effort for a global application.

Continuum is a continuous distributed hydrological model that relies on a morphological approach, based on drainage network components identification (Giannoni et al., 2000; Giannoni et al., 2005). These components are derived from DEMs. The DEM resolution drives the model spatial resolution. Flow in the soil is divided firstly into a sub-surface flow component that is based on a modified Horton schematization (see Gabellani et al., 2008 for details) and that follows the drainage network directions; and secondly, into a deep flow component that moves following the hydraulic head gradient obtained by the water-table modeling. The surface flow schematization distinguishes between channel and hillslope flows. The overland flow (hillslopes) is described by a linear reservoir scheme, while for the channel flow (channel) a schematization derived by the kinematic wave approach (Wooding, 1965; Todini and Ciarapica, 2001) is used. The energy balance is solved explicitly at cell scale by means of the force-restore equation, that allows having the LST as a distributed state variable of the model (e.g., Lin, 1980; Dickinson, 1988; Sini et al., 2008). The snow accumulation-melting module is a simple model that is derived from commonly used equations (Maidment, 1992) and it is forced by meteorological observations. The mass balance is applied at cell scale for the entire domain of the model, so that a snow cover map can be generated with the same resolution of the DEM. The energy balance and, as a consequence, the evapotranspiration are inhibited for those cells where snow cover is present. The applied approach is very simple and neglects the heat exchanges between the soil and the snow cover, but it is generally sufficient if the goal is the estimation of the snow contribution to the runoff. The precipitation is partitioned into solid or liquid if the air temperature is below or above a fixed threshold (Silvestro et al., 2015). For further details on the model please refer to Silvestro et al. (2013) and (2015).

Input Data for the hydrologic Simulations

For practical reasons, mainly computational constraints in the time span of the project, only one Global Climate Model was selected to drive the hydrological model. The GCM was used also for the representation of the present climate conditions considering the full Hydro-meteorological chain that includes the GCM forcing, the downscaling routines and the hydrologic model as a single model suit to be properly bias corrected and calibrated to reproduce the present climate statistics. This philosophy was preferred to the one making use of the reanalysis in present climate and subsequent calibration of the hydrologic model that would consider the Hydrologic model as a separate part with respect to the other chain

components. In this way the calibration procedure would tend to correct for biases caused by the full modelling chain application.

The EC-Earth model was selected for different reasons. First is base on one of the most advanced NWP currently available and targets a seamless prediction philosophy exploiting much of the experience gathered in short to medium-term forecast that are of incomparable value for extremes prediction. Second the CIMA Foundation research group has tight research cooperation with the EC-Earth community, which eases insights into the model runs and data accessibility, as well as continuous exchange on the simulation reliability with the developers.

The NWP system of the European Centre for Medium-Range Weather Forecasts (ECWMF) forms the basis of the EC-Earth Earth-system model (hence the name EC-Earth). The atmospheric model of EC-Earth version 2, is based on ECMWF's Integrated Forecasting System (IFS), cycle 31R1, corresponding to the current seasonal forecast system of ECMWF. The standard configuration runs at T159 horizontal spectral resolution with 62 vertical levels. In fact, some aspects of a newer IFS cycle have been implemented additionally, including a new convection scheme and the new land surface scheme H- TESSEL. The ocean component is based on version 2 of the NEMO model, with a horizontal resolution of nominally 1 degree and 42 vertical levels. The sea ice model is the LIM2 model. The ocean/ice model is coupled to the atmosphere/land model through the OASIS 3 coupler. Version 3 of the EC-Earth model outputs has been used here.

The EC-Earth runs in present climate spans from 1960 to 2012.

The meteorological forcing fields needed to run the model simulation are:

- Precipitation
- Temperature field at 2 meters
- Wind field (horizontal components)
- Incoming Net Radiation (long- and short-wave component)
- Atmospheric humidity at 2 m level

Precipitation and tempearture fields are amog the above forcing set the most impacting for flood simulation governing the determination of Initial and boundary conditions for the hydrologic model.

Therefore a bias correction tho these fields was performed, after comparison with observed quantities, in order to ensure proper results in present climate an a reliable calibration of the hydrologic model.

Bias Correction of the EC-Earth rainfall dataset

An analysis of the rainfall dataset obtained by the EC-Earth model simulation, based on the ECMWF Seasonal Forecasting System, was compared with a global dataset of observed precipitation, CHIRPS. The simulation taken into consideration was open-loop (without assimilation), with the simulated period ranging from 1960 to 2012. Only statistical characteristics of the simulated rainfall were considered in the comparison. The CHIRPS dataset is constituted by a merging of satellite-measured rainfall and ground rain gauges

network, it covers the period 1981-2012 and it is spatially limited to the band of the land between 50° of South Latitude and 50° of North Latitude. The comparison with the EC-Earth rainfall dataset was then limited to this spatial extent and to the period 1981-2012.

Dataset description and statistics comparison

EC-Earth

Timestep: 3 hours

Spatial resolution: 1.125°

Coverage: global (Longitude: -180° - +180° , Latitude: -90° - +90°)

CHIRPS

Timestep: pentadal (each month is subdivided in 5 periods of 5 days each and a sixth period of variable length)

Spatial resolution: 0.05° (approximately 5 km)

Coverage: land (Longitude: -180° - +180° , Latitude: -50° - +50°)

A comparison of the main statistics (mean, standard deviation, coefficient of variation) was also performed. In general, it can be noted how the EC-Earth dataset tend to distribute the rainfall height towards higher latitudes, with respect to CHIRPS, in which the precipitation volumes are more concentrated in the tropical band.

For the comparison the EC-Earth data were aggregated at the same pentadal time-step of CHIRPS. The analysis was limited to the CHIRPS spatial extent.

Maps and time series comparison

A comparison between the maps of yearly precipitation and of the monthly time-series is shown in Figures 1-4. It can be noted that the error between the two datasets presents quite defined spatial patterns, being mainly concentrated in the equatorial and tropical regions, while an analysis of the time series shows a significant difference in the variance, mainly due to the underestimation of the summer precipitations.

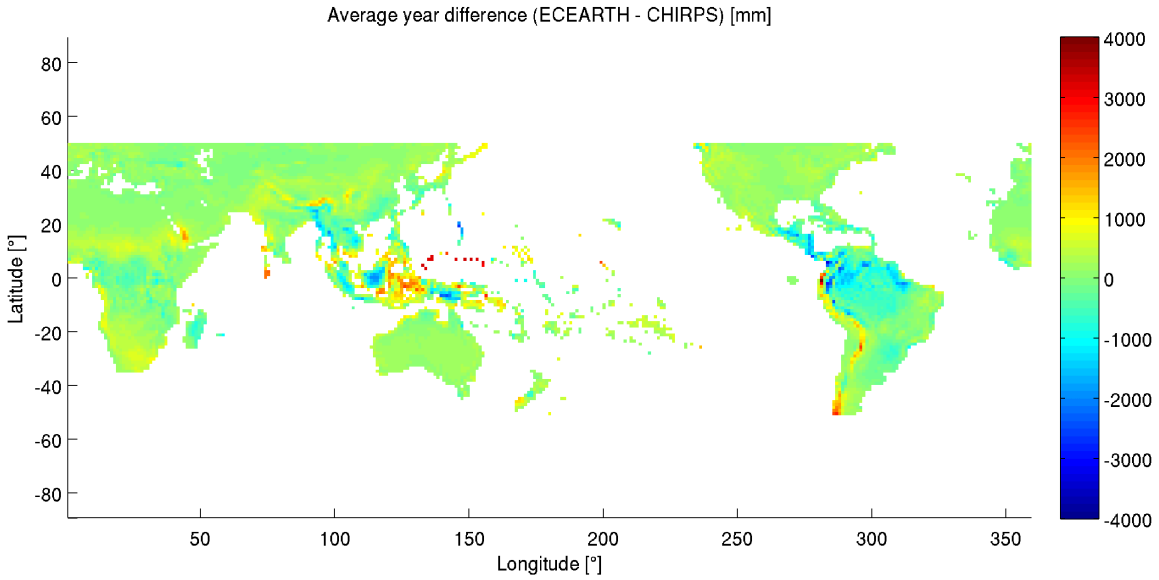

Figure 37 Difference of the yearly average precipitation (EC-Earth – CHIRPS). The mean difference of the total volume is about 3% (EC-Earth underestimates CHIRPS).

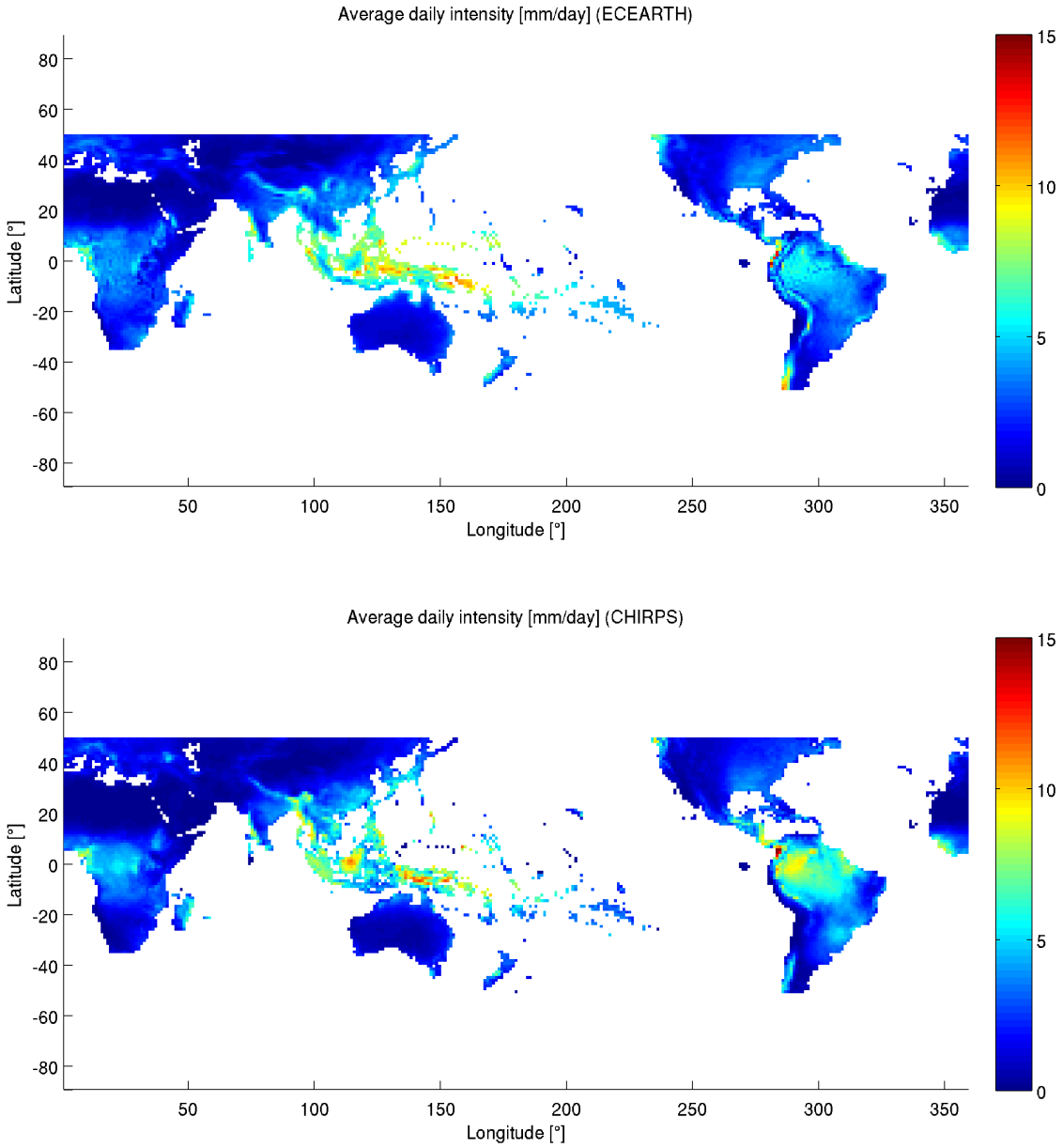

Figure 38 Comparison of the average daily intensities for each cell. Top panel: EC-Earth, bottom panel: CHIRPS.

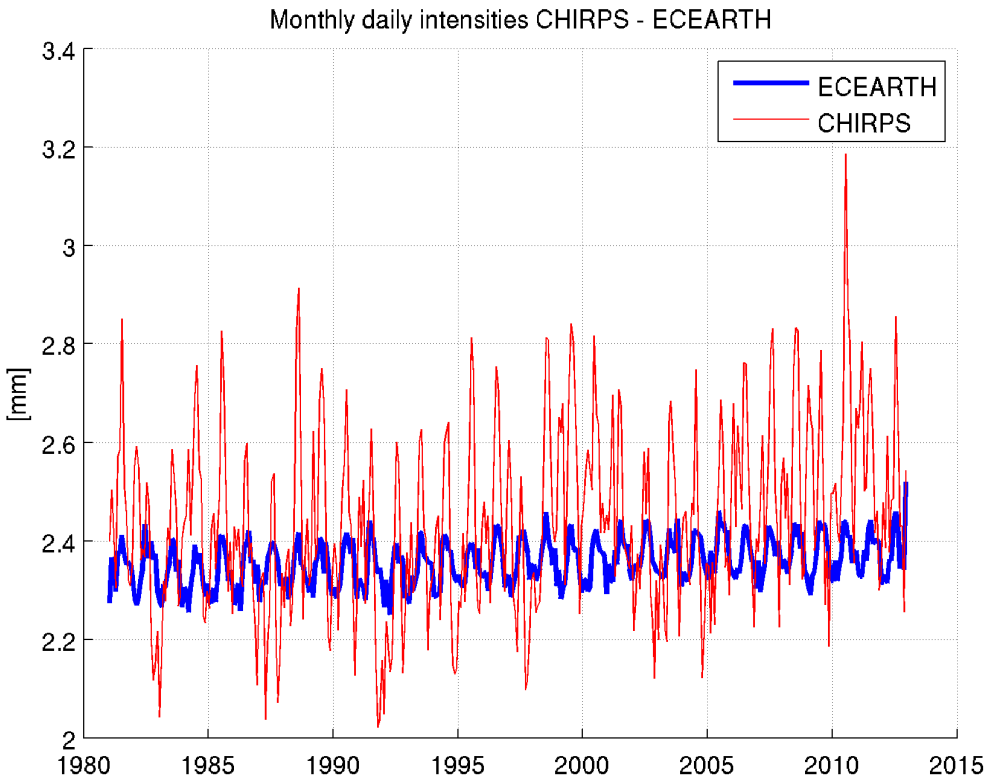

Figure 39 Comparison of the daily intensities time series (monthly and global average). It is evident that the EC-Earth variance is much lower with respect to the CHIRPS dataset.

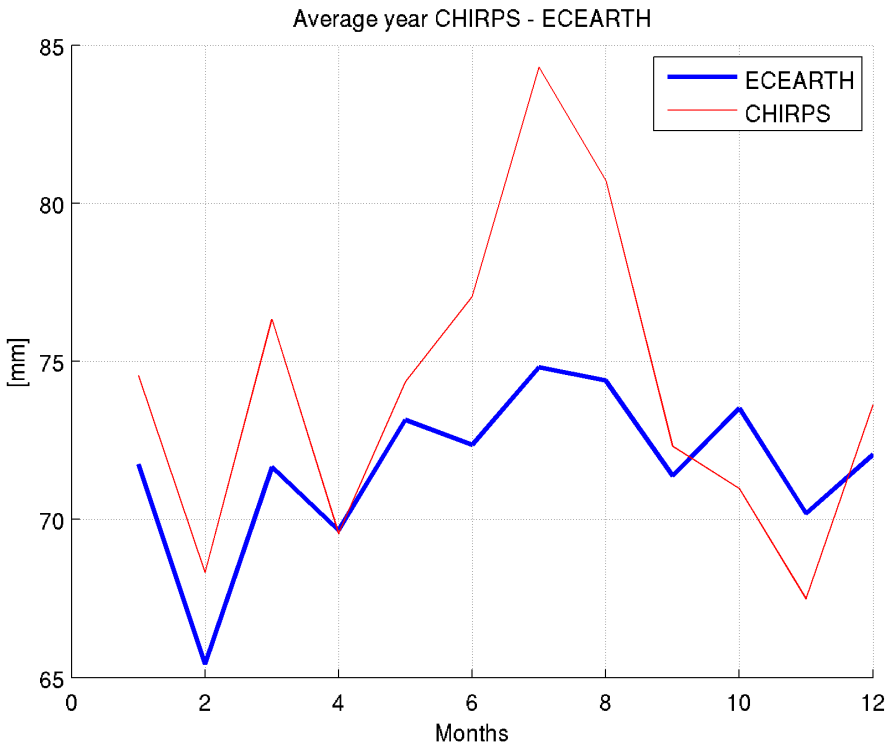

Figure 40 Comparison of the average year. It is evident a seasonality in the error between EC-Earth and CHIRPS dataset.

Bias Correction

In order to make the rainfall dataset to match at least the main statistical characteristics of the CHIRPS dataset (that was compared independently with rainfall observations, yielding an average error less than 4% on yearly basis in North America), a correction of the EC-Earth precipitation values was performed.

A simple additive correction was not possible; to avoid the creation of negative values, furthermore there was the need to preserve the rainfall-no rainfall structure of the EC-Earth dataset, given the pentadal aggregation of CHIRPS data. Furthermore, due to the significant differences in terms of spatial patterns (Figure 2), the correction was to be carried on a cell basis, in order to reproduce the CHIRPS distribution of the rainfall volume, especially at the different Latitudes.

An initial attempt to impose, on annual basis, the mean and the variance of the annual time series per cell was discarded, because of the problems of imposing both statistical moments and maintaining at the same time the positivity of the variable and the zeros structures of the 3-hours time series.

The final correction was done by imposing the monthly mean of the CHIRPS dataset on a cell basis. More precisely, at the purpose of preserving an inter-annual variability, the following correction was imposed for each cell and for each 3-hours value of the EC-Earth rainfall:

$$P_{EC-Earth,i}(t) = P_{EC-Earth,i}(t)\frac{PM_{CHIRPS}(m)}{PM_{EC-Earth}(m)} \quad (1)$$

where:

$P_{EC\text{-}Earth,i}(t)$ = 3-hours EC-Earth precipitation on the cell i, at the time t

$PM_{EC\text{-}Earth}(m)$ = EC-Earth monthly cumulated precipitation for the average month m (average on the whole period 1981-2012) in which the time t falls

$PM_{CHIRPS}(m)$ = CHIRPS monthly cumulated precipitation for the average month m (average on the whole period 1981-2012) in which the time t falls

The monthly-based correction allowed to deal with the strong summer underestimation shown in Figure 4, and to preserve the same sub-pentadal rainfall structure of EC-Earth (not available in CHIRPS data).

Due to the limited spatial extend of the CHIRPS dataset, another problem arose on how to correct the regions above and below 50° of Latitude North and South. Given the decreasing of the differences between CHIRPS and EC-EARTH datasets observed with the latitude (the maximum differences are observed at the Equator), a linear correction was applied in the areas between 50° and 60° of latitude, North and South.

In particular, for each month and for each longitude, the correction was applied by linear extrapolation on the ratio between the monthly value of the cell at 50° and the average of the whole column of cells at constant longitude; then, this correction factor, computed for each cell in the band 50°-60°, was employed for reconstruct the corresponding rainfall values. The correction was computed with the constraint of the continuity with the CHIRPS-corrected maps for each longitude at 50° of Latitude and the positivity of the final corrected rainfall values. Applying this method to all months and all cells in the 50°-60° bands, no significant longitudinal discontinuities were observed.

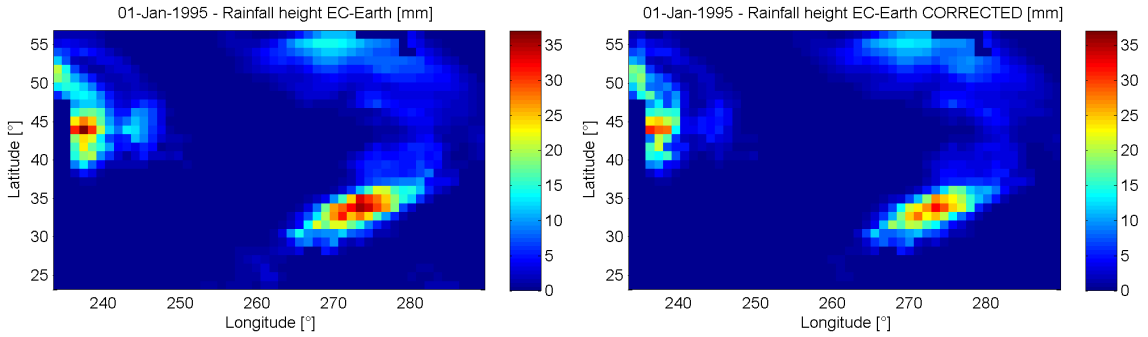

Figure 41 Comparison between rainfall patterns (one instant in time) – Original EC-Earth output (left panel) and Bias corrected pattern (right panel). Domain: North America.

Bias Correction of the EC-Earth temperature dataset

Similarly to Rainfall, an analysis of the temperature at 2-m dataset obtained by the EC-Earth model simulation, was compared with a global dataset of observed temperature, CRU-TS 3.21 dataset. The simulation taken into consideration was open-loop (without assimilation), with the simulated period ranging from 1960 to 2012. Only statistical characteristics of the simulated Temperature were considered in the comparison.

Unlike rainfall, in case of temperature a pixel-by-pixel additive correction was chosen that preserves the 3-hourly structure of the EC-Earth simulated fields.

The correction equation used is then:

$$\widetilde{T}_i(t) = T_i(t) + \left(T_{iCRU,m} - T_{iE,m}\right)$$

where:

$T_i(t)$ = temperature of the pixel i at the time t

$T_{iCRU,m}$ = average monthly CRU temperature of the pixel i for the average month m (m=1,…,12)

$T_{iE,m}$ = average monthly EC-Earth temperature of the pixel i for the average month m (m=1,…,12)

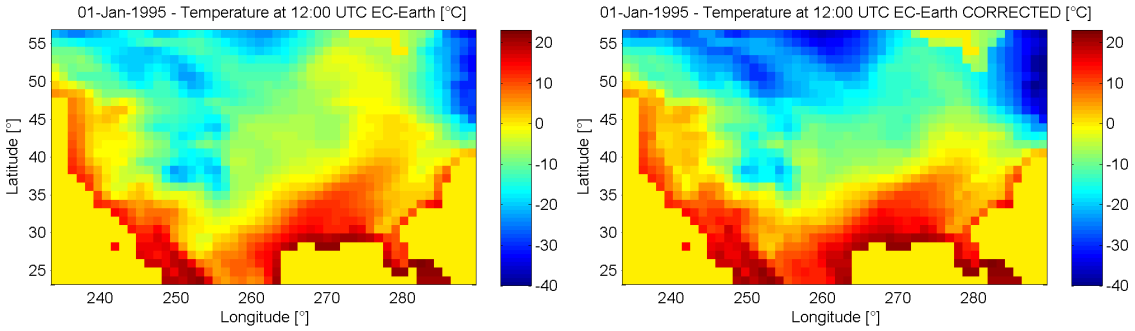

Figure 42 Comparison between a temperature patterns at 2 m (one instant in time) – Original EC-Earth output (left panel) and Bias corrected pattern (right panel). Domain: North America.

Downscaling the meteorological variables

Once the bias correction has been performed, a proper downscaling procedure of the EC-Erath fields is needed in order to properly prepare the inputs for the hydrological model.

The hydrologic model has been implemented on an aggregation of the reconditioned Hydroshed DEM at a scale of 7 km by 7 km on the global domain. Such scale is a balance between the need of properly representing the processes and the catchment features (e.g. the drainage network) and the need of maintaining as low as possible the computational load.

The EC-Earth fields are available at 1.125° resolution and need to be downscaled at the hydrologic model resolution. The impact of downscaling has been discussed in literature and here is faced in the best possible way considering the global application.

Each meteorological variable is downscaled in a different way in order to maintain as realistic as possible the small-scale features at the Hydrologic model resolution.

- Rainfall is the most complex, and impacting, variable to be downscaled. Here a filtered autoregressive model named RainFARM® has been used (Rebora et al., 2006). The Rainfall Filtered Autoregressive Model (RainFARM), is based on the nonlinear transformation of a Gaussian random field, and it conserves the information present in the rainfall fields at larger scales. The rainfall fields of EC-Earth have been downscaled to a temporal resolution of 1 hour and to the spatial resolution of 7-by-7 km.
- Temperature is quite sensitive to height variations that are represented at the finer scale. Therefore the Temperature field has been re-gridded on the finer grid as follow: EC-earth Temperature field has been assigned to barycentre DEM cell, then it is Rescaled on other DEM cells using and adiabatic lapse rate (i.e. 0.649°/100 m)
- Radiation has been re-gridded taking into consideration the shadowing effect at finer scale using the simplified algorithm from Dozier and Frew, 1990.
- Relative humidity has been re-gridded starting from dew-point temperature re-grid following a procedure similar to the temperature field but using the humid adiabatic lapse rate (i.e. 0.4°/100 m). Then, the Relative humidity has been computed as a function of both re-gridded Temperature and re-gridded dew point Temperature.
- For wind components a simple re-gridding of the wind field values has been performed.

Hydrologic model calibration and simulation results

Once the meteorological fields have been bias corrected, downscaled and prepared for the run on a global scale the calibration procedure of the Hydro-meteorological chain has been set. The first step is to reduce as much as possible the calibration parameter and constrain them in a physically meaningful domain.

Various authors highlighted the importance of reducing the model parameterization and maintaining a stable and simple structure (Montaldo et al., 2005; Coccia et al., 2009; Todini, 2009; Brocca et al., 2011b). The design of Continuum follows the philosophy of finding a balance between a detailed description of the physical processes and a robust and parsimonious parameterization.

Some parametric variables are derived from ancillary information (e.g. morphological parameters from DEM analysis (Giannoni et al. 2005) or the storage capacity of the vegetation parameterized using the Leaf Area Index (LAI) as in Kozak et al., 2007), while other need to follow a standard input – output calibration.

Continuum has six parameters that need calibration at basin scale: two for the surface flow, two for the sub-surface flow and two for deep flow and the water table. In Table 1 the calibration parameters are listed and linked to the physical processes parameterized.

Parameter	**Description**
u_h [s^{-1}]	Flow motion coefficient in hillslopes
u_c [$m^{0.5}s^{-1}$]	Friction coefficient in channels
c_f [-]	Defines the infiltration capacity at saturation
c_t [-]	Defines the mean field capacity
R_f [-]	Related to anisotropy between the vertical and horizontal saturated conductivity, and to soil porosity
V_{Wmax} [mm]	Maximum water capacity of the aquifer on the whole investigated area

Table 2 Model parameters schematic description

The hillslope flow motion parameter u_h influences the general shape of the hydrograph, while the impact of u_c on the hydrograph shape depends on the length of the channeled paths. These are two lumped parameters: u_c represents the friction coefficient in the channel motion equation, u_h accounts for the general characteristics of the hillslope that influence the motion (e.g. friction, slope) and is more an empirical parameter.

The parameter c_t is related to the soil field capacity V_{fc} and identifies the fraction of water volume in the soil that can be extracted only through evapotranspiration. The relationship is:

$$V_{fc} = c_t V_{\max} \quad (1)$$

Where V_{max} is the maximum capacity of the soil to storage water in the root zone.

The "infiltration capacity" parameter c_f controls the velocity of subsurface flow (i.e, it is related to saturated hydraulic conductivity), defining the asymptotic minimum infiltration rate for saturated soils f_1 with the following equation:

$$f_1 = c_f f_0 \quad (2)$$

Where f_0 is the maximum infiltration rate for completely dry soil.

The parameters c_t and c_f regulate the dynamics of saturation at cell scale. Since both f_0 and V_{max} are distributed parameters estimated as functions of Curve Number (Gabellani et al., 2008) the pattern of f_1 and V_{fc} is spatially modulated by the pattern of Curve Number maps (Silvestro et al., 2013), which are a synthetic representation of the local soil properties.

The parameters V_{Wmax} and R_f govern the deep flow and the water table dynamic (Silvestro et al., 2013). V_{Wmax} represents the absolute maximum water content of the aquifer on the whole investigated area, the maximum water content on each cell is estimated basing on V_{Wmax} and on the slope (Saulnier et al., 1997). R_f is a multiplicative factor in the Darcy equation used to estimate the flux per unit area between two contiguous cells and mainly takes care of differentiating the saturated vertical and horizontal conductivity. These two parameters have a reduced influence compared to the other four parameters because of the slow temporal dynamic of the water table. The sensitivity to R_f increases with the total basin drainage area when the effect of the interaction between the water table and the vadose zone becomes crucial in the formation of the recession curve between the rainfall events (Silvestro et al., 2013).

The Curve Number map that is used as a basis to derive most of the soil properties is one of the most impacting steps of the procedure. Given the uncertainty in deriving a Curve Number map at global level the following calibration strategy was applied.

The Hydrologic model was set up with standard values for the 6 above mentioned parameters and the Curve Number map was calibrated in order to obtain the best results in terms of quantiles statistics in the gauged sections in the different global domains. Once the best calibration value was reached (CN values constrained to assume physically reasonable values with respect to land use and soil type information available) the remaining 6 parameters were calibrated in order to improve the quantiles matching. The procedure was iterated twice.

Regarding the CN calibration each section was calibrated independently. In case of nested sections the upstream ones were calibrated first and the downstream ones were used to calibrate the incremental part of the territory only. The cost function applied is based on the RMSE computed on ten reference quantiles over 95% (extremes led calibration). In order to reduce the computation time an efficient 1-D polynomial line search strategy was implemented for the optimisation of the model runs.

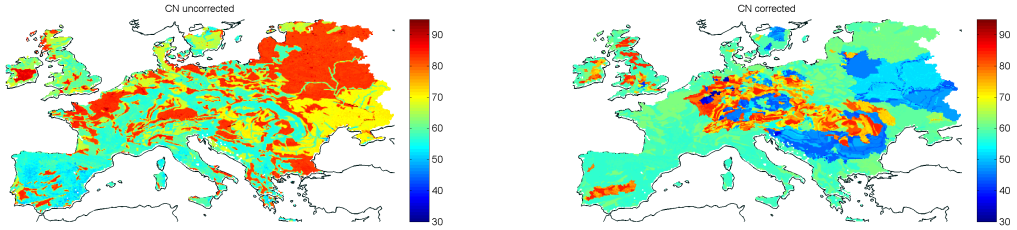

Figure 43 CURVE Number map for one of the computation domains (Europe). Left panel original CN map, Right Panel calibrated CN map

The calibration procedure was computationally intensive therefore the procedure was highly parallelized and run on SUPERMUC: Leibniz Supercomputing Centre in Garching (Munich), were more than 500 cores were used simultaneously with over 100 hours computation time.

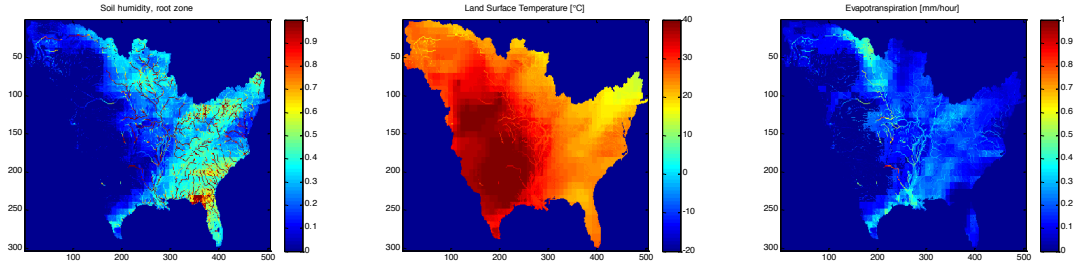

Figure 44 output fields produced by the model : Soil Humidity, Land Surface Temperature, Evapotranspiration. Domani : Noth America – USA

It is important to note that all Dams identified as influential have been implemented in the model with their own geometrical parameters. Since no management rule was known, the no-management rule (i.e. no release if not the normal one during flood events or preceding a flood event) has been applied. In case the dam was meant for flood lamination maximum lamination strategy has been applied in that case.

After the calibration procedure has been performed the model outputs have been spot-checked for physical consistencies. An example of the checked fields is reported in Figure 44 for one specific timeframe of the run.

Results of the procedure have been statistically tested at sincle gauging sections (…) and on a regional level with respect to the growth curve obtained by observations. Results (especially when the regional growth curve is analised) are stisfactory in all domains and in most of the gauged sections, passing the KS test at 95% level in more than 95% of the cases.

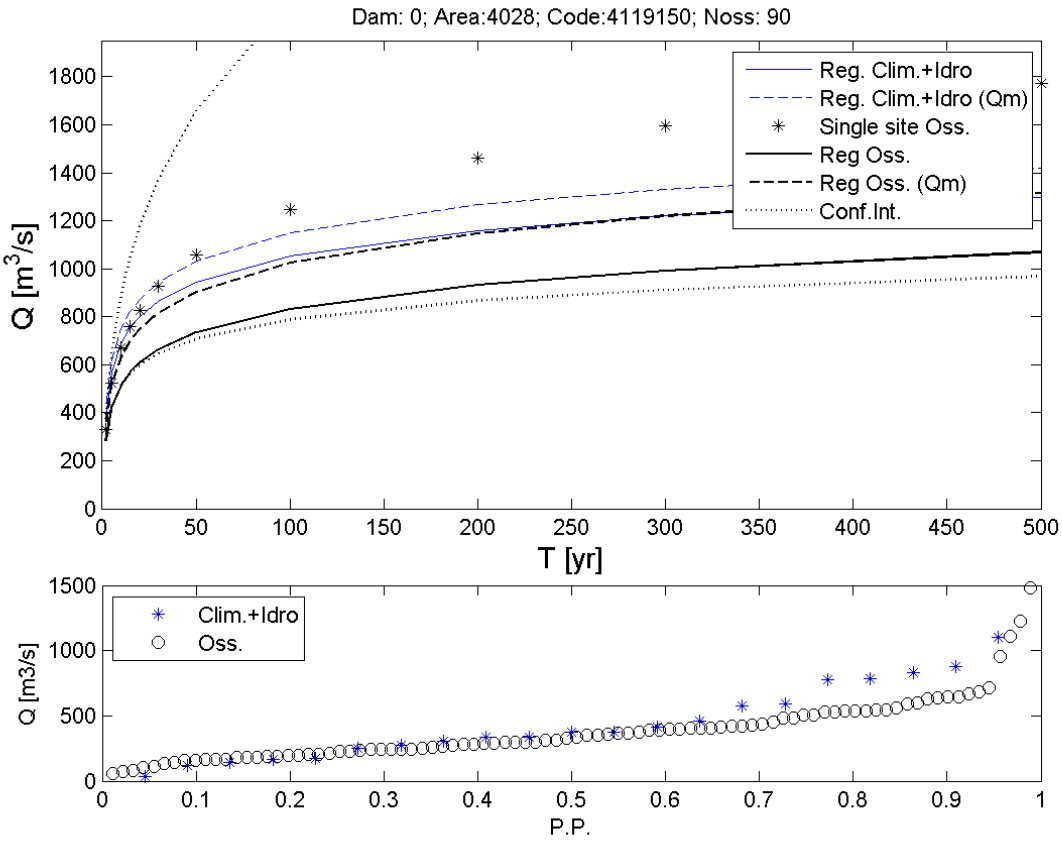

Figure 45 the figure present the result for one section in USA with more tha 90 years of observations. Legend upper panel: Conf. Int. (confidence interval at 0.05 significance level), Reg. Oss. (Qm) (regional Growth Curve from observations – rendered dimensional using local average mean from observations), Reg. Oss. (regional Growth Curve from observations – rendered dimensional using discharge index from regression), Single Site Oss. (single site observation points), Reg. Clim. + Idro (Qm) (regional Growth Curve from Model simulations – rendered dimensional using local average mean from observations), Reg. Clim. + Idro (regional Growth Curve from Model simulations – rendered dimensional using discharge index from regression). Lower panel shows a PP plot comparing observation and model simulations.

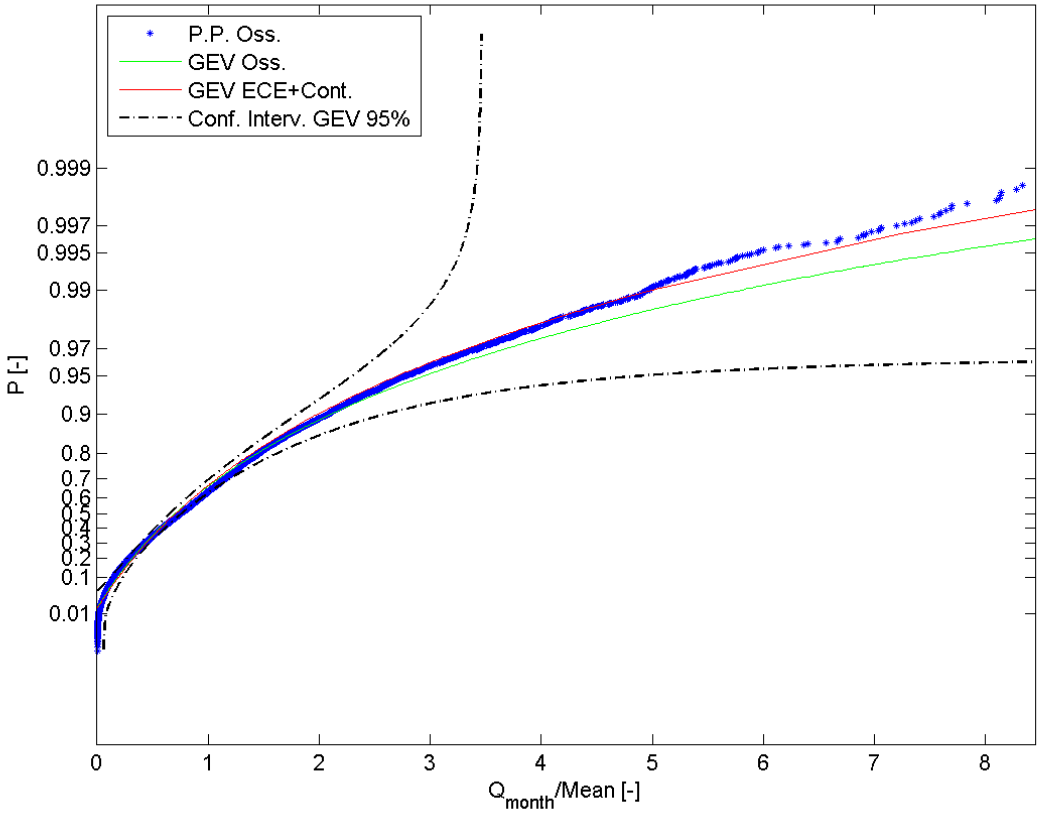

*Figure 46 Growth curve for a domain with **Tempered Climate** comparioson between simulations and observations. Legend : P.P. Oss. (Observations Plotting position points), GEV Oss. (Generalised Extreme value distribution growth curve from observations), GEV ECE+Cont (Generalised Extreme value distribution growth curve from simulations EC-Earth + Continuum model), Conf. Interv GEV 95% (Confidence interval on the GEV from Observation at 0.05% significance level).*

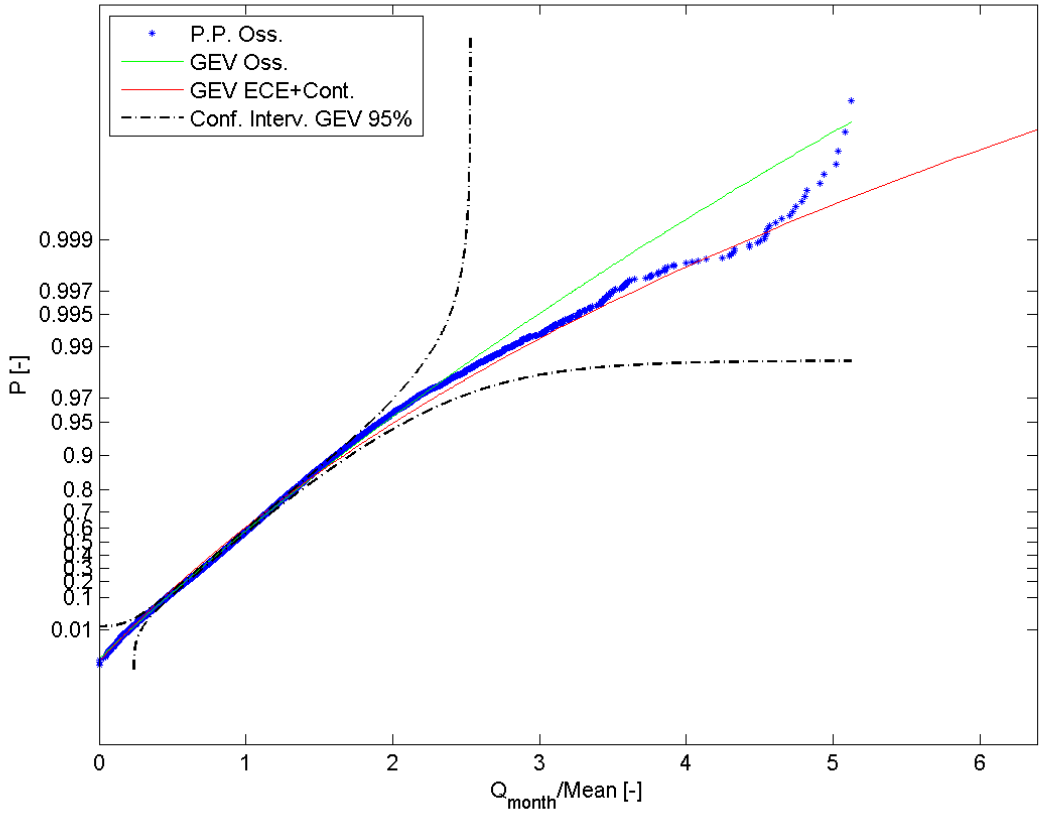

*Figure 47 Growth curve for a domain with **semi-arid Climate** comparioson between simulations and observations. Legend : P.P. Oss. (Observations Plotting position points), GEV Oss. (Generalised Extreme value distribution growth curve from observations), GEV ECE+Cont (Generalised Extreme value distribution growth curve from simulations EC-Earth + Continuum model), Conf. Interv GEV 95% (Confidence interval on the GEV from Observation at 0.05% significance level).*

Hydrological model runs in climate changed conditions

With the hydro meteorological chain calibrated in the present climate to properly reproduce the annual peak stream flow statistics one run in climate changed conditions has been performed following the same modelling chain used to perform the present climate runs. Due to time and computational constraints it was decided to run only one climate change scenario: the study used as reference the RPM4.5 scenario as it is considered the most probable so far.

EC-earth variables have been prepared and fed to the Hydro model after applying the same bias correction used for the present climate run on precipitation and temperature fields and after appropriate downscaling as previously described. Results obtained have been treated as mock observations and the statistical analysis to derive the regional growth curve have been applied to the simulated series.

After that a statistical comparison has been performed between the regional growth curves in present climate and in future climate in near future and far future. The results obtained so far are only preliminary and should be further analysed and validated. However the importance of attaching a detailed hydrologic simulation to the global climate runs has can

be highlighted. In Figure 48 the statistical comparison between two areas is shown. The first panel presents the results for a stream section in the Amazon basin. In this case the two regional curves for the site (the one in present climate and the one in Changed climate in the period 2010-2050) fall both within the confidence interval (significance level 0.05%) drawn around the curve derived directly from observed stream-flow values (sample size 31 years). In the second case for a stream section in South East Asia, the curve in climate change conditions falls out of the confidence limit showing significant change in the stream-flow annual maxima time series.

Both areas were highlight as wet anomalies also in the IPCC SREX report. However after the application of the hydrologic model such anomaly is smoothed (if not reduced) in the case of the amazon basin while it is enhanced in the case of the South East Asian domain.

As already said these result are preliminary and should not by any means used as a reference by now, but the message is clear that even for global application a proper hydrological modelling is necessary to increase the information content of climate projections.

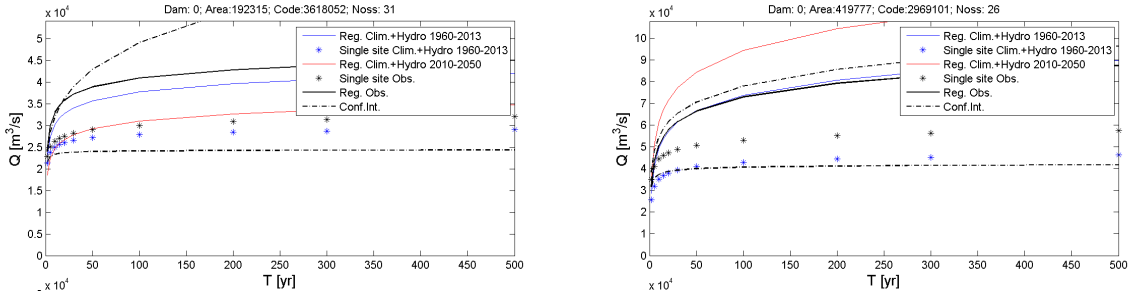

Figure 48 the left panel shows results for the Amazon basin: all curves are contained within the confidence limits; the right panel shows results for one section in the South east Asia domain: in this case the regional curve (in red) falls outside the confidence limits showing a clear increase of extremes frequency.

Conclusions

A methodology for deriving Hazard maps on the global level has been introduced. Such methodology, unlike many others relaying mainly on precipitation fields, puts emphasis on the use of stream flow data directly, and gives credible results in terms of hazard and risk computation. Preliminary results have been also presented in terms of changed risk in a changed climate. The Hydrologic model implementation serves as a basis for the CC simulation, but also to derive fundamental information for the improvement of the results far from gauged sections. Continuous stream flow simulation is also at the heart of the methodology for the development of flood scenarios, to be used in the full probabilistic risk assessment. This part of the work is still under validation and will be presented and described later this year.

References

Arcement, G.J., Schneider, V.R., 1989. Guide for selecting Manning's roughness coefficients for natural channels and flood plains. US Geological Survey, Water Supply Paper No. 2339.

Basu, B., & Srinivas, V. V. (2014). Regional flood frequency analysis using kernel-based fuzzy clustering approach. Water Resources Research, 50(4), 3295-3316.

Biswas, A.K. & Fleming, G. (1966) Floods in Scotland: magnitude and frequency. Wat. Wat. Engng, 246-252.

Bobe´e B, Rasmussen PF, Recent advances in flood frequency analysis. U.S. National Report to IUGG, 1991‐1994, Rev. Geophys., 1995; 33(Suppl.):1111‐6.

Bocchiola, D., De Michele, C., and Rosso, R., (2003), Review of recent advances in index flood estimation, Hydrol. Earth Syst. Sci., 7, 283-296.

Boni, G., Ferraris, L., Giannoni, F., Roth, G., & Rudari, R. (2007). Flood probability analysis for un-gauged watersheds by means of a simple distributed hydrologic model. Advances in water resources, 30(10), 2135-2144.

Bougthon W, Droop B. Continuous simulation for design flood estimation ‐ a review. Environ Model Software 2003;18:309‐18.

Bras RL. Hydrology an introduction to hydrologic science. Addison-Wesley; 1990.

Burn D., H., Catchment similarity for regional flood frequency analysis using seasonality measures, Journal of Hydrology 202, 212–230, 1997.

Brunner, G. W. 2008. "HEC-RAS, River Analysis System hydraulic Reference Manual. US Army Corps of Engineers, Hydraulic Engineering Center USACE HEC". 411Davis.

Chong, S. & Moore, S.M. (1983) Flood frequency analysis for small watersheds in southern Illinois. Wat. Resour. Bull. 19(2), 277-282.

Chow VT, Maidment DR, Mays LW. Applied hydrology. McGraw-Hill; 1988. p. 444‐70.

Climatic Research Unit (CRU) time-series datasets of variations in climate with variations in other phenomena. University of East Anglia Climatic Research Unit (CRU). [Phil Jones, Ian Harris]. CRU Time Series (TS) high resolution gridded datasets, [Internet]. NCAS British Atmospheric Data Centre, 2008, *Date of citation*. Available from http://badc.nerc.ac.uk/view/badc.nerc.ac.uk__ATOM__dataent_1256223773328276

Cole, G. (1966) An application of the regional analysis of flood flows. In: Symposium on River Flood Hydrology, Session B, 39-57. Institution of Civil Engineers, London.

Dalrymple, T. (1960) Flood frequency analyses. US Geol. Surv. Wat. Supply Pap. 1543-A.

Dickinson, R., (1988) The force-restore method for surface temperature and its generalization, *Journal of Climate*, 1:1086-1097.

Dozier, J., Frew J. (1990) Rapid calculation of terrain parameters for radiation modeling from digital elevation data, IEEE Trans. Geosci. Remote Sens., 28 (5), pp. 963‐969

Giannoni, F., Roth., G., Rudari, R., (2000) A Semi – Distributed Rainfall – Runoff Model Based on a Geomorphologic Approach, *Physics and Chemistry of the Earth*, 25/7-8, 665-671.

Giannoni, F., Roth., G., Rudari, R., (2003) Can the behavior of different basins be described by the same model's parameter set? A geomorphologic framework, *Physics and Chemistry of the Earth*, 28, 289–295.

Giannoni, F., Roth., G., Rudari, R., (2005) A procedure for drainage network identification from geomorphology and its application to the prediction of the hydrologic response, *Advances in Water Resources*, 28, 6, 567-581.

Gabellani, S., Silvestro, F., Rudari, R., Boni, G., (2008) General calibration methodology for a combined Horton-SCS infiltration scheme in flash flood modeling, *Nat. Hazards Earth Science*., 8, 1317 - 1327.

Gabriele S, Arnell NW. A hierarchical approach to regional flood frequency analysis. Water Resour Res 1991;27(6):1281‐9.

Global Land Cover 2000 database. European Commission, Joint Research Centre, 2003. http://gem.jrc.ec.europa.eu/products/glc2000/glc2000.php; BARTHOLOME, E. M. and BELWARD A. S., 2005, GLC2000; a new approach to global land cover mapping from Earth Observation data, International Journal of Remote Sensing, *26*, 1959 - 1977.

Hosking, J.R.M. and J.R. Wallis, 1993: Some statistics useful in regional frequency analysis. Water Resourc. Res., 29, 271-281

Katz, R. W., Parlange, M. B., Naveau P. (2002): Statistics of extremes in hydrology, Advances in Water Resources, 25, 1287–1304

Kottegoda NT, Rosso R. Statistics, probability and reliability for civil and environmental engineers. McGraw-Hill; 1997.

Lehner, B., C. Reidy Liermann, C. Revenga, C. Vorosmarty, B. Fekete, P. Crouzet, P. Doll, M. Endejan, K. Frenken, J. Magome, C. Nilsson, J.C. Robertson, R. Rodel, N. Sindorf, and D. Wisser. 2011. Global Reservoir and Dam Database, Version 1 (GRanDv1): Dams, Revision 01. Palisades, NY: NASA Socioeconomic Data and Applications Center (SEDAC).

Lehner, B. and Döll, P. (2004): Development and validation of a global database of lakes, reservoirs and wetlands. Journal of Hydrology 296/1-4: 1-22.

Lehner, B., Verdin, K., Jarvis, A. (2008): New global hydrography derived from spaceborne elevation data. Eos, Transactions, AGU, 89(10): 93-94.

Lin, J., D., (1980) On the Force-Restore method for prediction of ground surface temperature, *Journal of Geophysical Research*, 85, 3251-3254.

Maidment, D., (1992) Handbook of Hydrology. McGraw-Hill, Inc.

Manfreda, S., Di Leo, M., and Sole, A.: Detection of Flood Prone Areas using Digital Elevation Models, J. Hydrol. Eng., posted ahead of print 3 January, doi:10.1061/(ASCE)HE.1943-5584.0000367, 2011.

Merz, R., & Blöschl, G. (2005). Flood frequency regionalisation—spatial proximity vs. catchment attributes. Journal of Hydrology, 302(1), 283-306.

Mitchell, T.D. and Jones, P.D., 2005: An improved method of constructing a database of monthly climate observations and associated high-resolution grids. *International Journal of Climatology* **25**, 693-712.

Peel, M. C., Finlayson, B. L., McMahon, T. A., Updated world map of the Koppen-Geiger climate classification, Hydrol. Earth Syst. Sci., 11, 1633–1644, 2007.

Rebora N, Ferraris L, von Hardenberg J, Provenzale A. (2006) RainFARM: Rainfall Downscaling by a Filtered Autoregressive Model. *Journal of Hydrometeorology* **7**(4): 724-738.

Shuttle Radar Topography Mission (SRTM) Near-global Digital Elevation Models (DEMs). Produced from a collaborative mission by the National Aeronautics and Space Administration (NASA), the National Imagery and Mapping Agency (NIMA), the German Aerospace Center (DLR, Deutsches Zentrum fur Luft-und Raumfart), and the Italian Space Agency (ASI, Agenzia Spaziale Italiana). Available for electronic download and on CD-ROM from the U.S. Department of the Interior, U.S. Geological Survey, Earth Resources Observation Systems (EROS) Data Center (EDC), Distributed Active Archive Center (DAAC), Sioux Falls, South Dakota, USA.

Silvestro, F, Gabellani S., Delogu F., Rudari R., and Boni G. (2013) Exploiting remote sensing land surface temperature in distributed hydrological modelling: the example of the Continuum model, Hydrol. Earth Syst. Sci., 17, 39-62, doi:10.5194/hess-17-39-2013

Silvestro, F., Gabellani, S., Rudari, R., Delogu, F., Laiolo, P., Boni, G., Uncertainty reduction and parameters estimation of a distributed hydrological model with ground and remote sensing data, Accepted for publication in Hydrol. Earth Syst. Sci. (2015)

Sini, F., Boni, G., Caparrini, F., Entekhabi, D., (2008) Estimation of large-scale evaporation fields based on assimilation of remotely sensed land temperature, *Water Resour. Res.*, 44, W06410, doi:10.1029/2006WR005574.

Saulnier, G. M., Beven, K., Obled, C., (1997), Including spatially variable effective soil depths in TOPMODEL, *Journal of Hydrology*, 202, 158-172

Todini, E., Ciarapica, L., (2001), The TOPKAPI Model. Mathematical Models of Large Watershed Hydrology. In: Singh, V. P. and Frevert, D. K., Water Resources Publications, Littleton, Colorado, Chapter 12.

Verdin, K.L., A System for Topologically Coding Global Drainage Basins and Stream Networks, Earth Resources Observation Systems (EROS) Data Center, 1997.

Wooding, R. A., (1965) A hydraulic modeling of the catchment-stream problem. 1. Kinematic wave theory, Journal of Hydrology, 3, 254–267.